NeuroImage 273 (2023) 120095

Contents lists available at ScienceDirect

NeuroImage

journal homepage: www.elsevier.com/locate/neuroimage

Relationships between neurotransmitter receptor densities and expression levels of their corresponding genes in the human hippocampus

Ling Zhao[a,1], Thomas W. Mühleisen[a,b,c,1], Dominique I. Pelzer[a], Bettina Burger[c], Eva C. Beins[d], Andreas J. Forstner[a,d], Stefan Herms[c,d], Per Hoffmann[c,d], Katrin Amunts[a,b], Nicola Palomero-Gallagher[a,b,2,*], Sven Cichon[a,c,e,2,*]

[a] Institute of Neuroscience and Medicine (INM-1), Research Centre Jülich, Germany
[b] Cécile and Oskar Vogt Institute for Brain Research, Medical Faculty, University Hospital Düsseldorf, Heinrich Heine University Düsseldorf, Germany
[c] Department of Biomedicine, University Hospital Basel and University of Basel, Switzerland
[d] Institute of Human Genetics, University of Bonn, School of Medicine & University Hospital Bonn, Bonn, Germany
[e] Institute of Medical Genetics and Pathology, University Hospital Basel, Switzerland

ARTICLE INFO

Keywords:
Rna expression
Receptor density
Human hippocampus
Genomic
Transcriptomic
Receptomic

ABSTRACT

Neurotransmitter receptors are key molecules in signal transmission, their alterations are associated with brain dysfunction. Relationships between receptors and their corresponding genes are poorly understood, especially in humans. We combined *in vitro* receptor autoradiography and RNA sequencing to quantify, in the same tissue samples (7 subjects), the densities of 14 receptors and expression levels of their corresponding 43 genes in the *Cornu Ammonis* (CA) and dentate gyrus (DG) of human hippocampus. Significant differences in receptor densities between both structures were found only for metabotropic receptors, whereas significant differences in RNA expression levels mostly pertained ionotropic receptors. Receptor fingerprints of CA and DG differ in shapes but have similar sizes; the opposite holds true for their "RNA fingerprints", which represent the expression levels of multiple genes in a single area. In addition, the correlation coefficients between receptor densities and corresponding gene expression levels vary widely and the mean correlation strength was weak-to-moderate. Our results suggest that receptor densities are not only controlled by corresponding RNA expression levels, but also by multiple regionally specific post-translational factors.

1. Introduction

Neurotransmitter receptors are membrane bound proteins or protein complexes which play vital roles in neuronal signaling transmission and thus constitute potential drug targets for the treatment of neurologic and neuropsychiatric disorders (Groc and Choquet, 2020; Zilles and Palomero-Gallagher, 2017). The central dogma of molecular biology postulates the major flow for the transfer of genetic information from DNA through RNA to protein. However, despite over two decades of research, the precise nature of the relationship between gene and protein/receptor expressions remains elusive particularly in the human brain, where only a few studies have been performed due to the limited brain tissue availability, technical challenges and high cost (Buccitelli and Selbach, 2020; Gry et al., 2009; Hansen et al., 2022a, 2022b; Zachlod et al., 2022).

Manifold biological regulation mechanisms drive the relationship between gene and protein expression levels in a complex manner (Buccitelli and Selbach, 2020; Gry et al., 2009; Hood and Emeson, 2011; Liu et al., 2016; Payne, 2015; Schulz et al., 2017; Vogel and Marcotte, 2012). Some examples of these mechanisms are the differential methylation at quantitative trait loci in the human hippocampus (Schulz et al., 2017), or the modification of protein properties by alternative exon selection (Keren et al., 2010). Furthermore, receptor assembly and trafficking (Fig. 1), which are specific features of neurotransmitter receptors (Collingridge et al., 2004; Groc and Choquet, 2020; Malinow and Malenka, 2002; Schwappach, 2008; Stephenson et al., 2008), make studies of the relationships between RNA expression levels and receptor densities most challenging. A notable example is the regulation of the subunit composition of NMDA receptors, encoded by *GRIN* genes, and trafficking at hippocampal synapses involved in plasticity (Ferreira et al., 2017; Paoletti and Neyton, 2007). However, dissecting correlations between genetic factors (e.g., gene transcription and translation) and receptor distributions in the human brain could provide novel insights into understanding the mechanisms of receptor

* Corresponding author at: Institute of Neuroscience and Medicine (INM-1), Research Centre Jülich, Germany.
E-mail addresses: n.palomero-gallagher@fz-juelich.de (N. Palomero-Gallagher), s.cichon@fz-juelich.de (S. Cichon).
[1] These authors contributed equally to this work.
[2] Joint senior authors.

https://doi.org/10.1016/j.neuroimage.2023.120095.
Received 16 November 2022; Received in revised form 2 March 2023; Accepted 5 April 2023
Available online 6 April 2023.

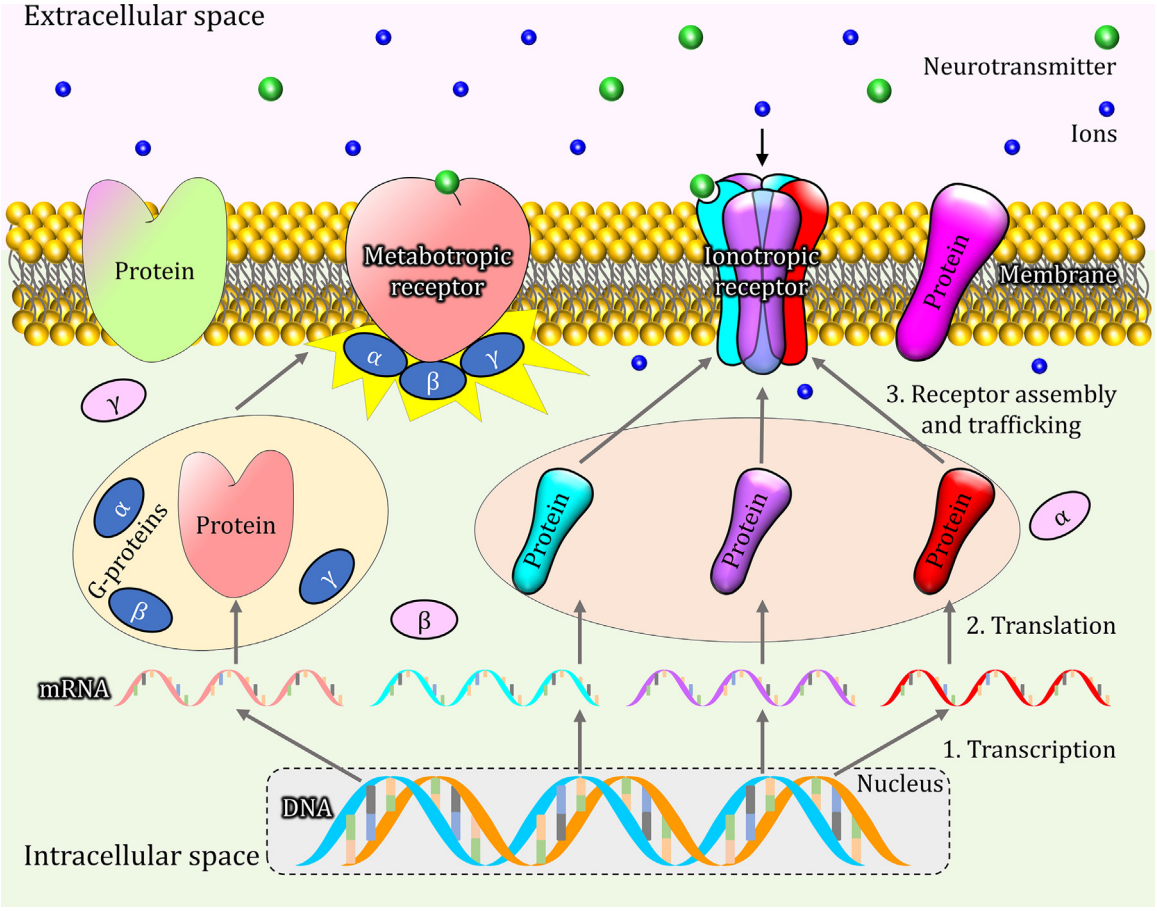

Fig. 1. A schematic diagram of the major steps involved in neurotransmitter receptor expression. The expression mechanisms are tightly controlled by gene transcription, translation, proper protein folding and co-assembly in the endoplasmic reticulum (ER), post-translational modifications, and subsequently trafficking to the appropriate membrane surface (on the cell body, dendritic tree or axonal bouton) along the secretory pathway (Levitz et al., 2016; Schwappach, 2008; Stephenson et al., 2008). Thus, the number of functional receptors is the result of several control steps more than those involved in protein synthesis. These additional steps include the complex control of receptor assembly from the single proteins, transport to the required site (trafficking) and dynamic inclusion in the cellular membrane. Of the receptors analyzed in the present study, the AMPA, NMDA, kainate, and $GABA_A$ belong to the ionotropic category, whereas mGluR2/3, M_1, M_2, M_3, α_1, 5-HT_{1A}, 5-HT_2, D_1, and A_1 are metabotropic.

expressions and span this necessary bridge to further understand the pathogenic mechanisms mediating the effects of genetic risk variants in neurologic and neuropsychiatric disorders.

Neurotransmitter receptors are heterogeneously distributed throughout the brain, and regional differences in receptor densities can be analyzed among others, by means of *in vivo* receptor positron emission tomography or of quantitative *in vitro* receptor autoradiography. While the first approach can be applied *in vivo* and is capable to capture dynamic changes of receptor binding in healthy and patient subjects, the latter method has the advantage of revealing specific regional and laminar distribution patterns of multiple receptors within the same brain sample and with a high resolution (Palomero-Gallagher and Zilles, 2018). Furthermore, *in vivo* neurotransmitter receptor imaging is only accessible for a limited set of receptor types due to both technical and ethical restrictions, which makes the *in vivo* visualization and quantification of multiple receptors in the same subject extremely difficult (Khan et al., 2021).

For receptor autoradiography, there is growing interest in comprehensively decoding the relationships between receptor densities and expression levels of their encoding genes across multiple regions of the human brain (Hansen et al., 2022a, 2022b; Murgaš et al., 2022; Zachlod et al., 2022). We recently performed correlation analyses of receptor densities and corresponding genes across 15 areas of the human primary and early visual, auditory, somatosensory, and motor cortices, and revealed a covariation of receptor densities with areal gene expression levels (Zachlod et al., 2022). Other studies encompassing 33–38 architectonically identified areas spread throughout the cerebral cortex revealed a lack of correlation for most of the analyzed receptor types (Hansen et al., 2022a; Murgaš et al., 2022). However, the spatial resolution of PET may obscure specific findings in single areas, and the RNA (Hawrylycz et al., 2012) and neurotransmitter receptor data (Zilles and Palomero-Gallagher, 2017) were obtained from different subjects. Inter-subject variability of RNA expression levels and of receptor densities superimposed on the effects of age differences may constitute a natural confounder to explore the relationship between these datasets (Murgaš et al., 2022), which cannot be fully overcome and compensated. Indeed, a pronounced interindividual variability of gene expression in the human hippocampus has been demonstrated in our previous study (Schulz et al., 2017).

The hippocampus plays a crucial role in functions including learning and memory, spatial navigation and emotion processing (Zhong et al., 2020). Notably, the hippocampus is also a key structure in various neurologic and neuropsychiatric disorders such as epilepsy and Alzheimer's disease (Berger et al., 2020; Bernasconi et al., 2003; Bernhardt et al., 2016, 2015; Blümcke et al., 2013; Debski et al., 2020; Hogan et al., 2004; Thom, 2014). The hippocampus consists of the dentate gyrus (DG) and the *Cornu Ammonis* (CA, with the CA1-CA3 regions) (Palomero-Gallagher et al., 2020). They are parts of the Papez circuit, which was proposed as the neuroanatomical substrate of emotion and memory (Aggleton et al., 2016; Papez, 1937). Information reaches the DG from

the entorhinal cortex through the perforant pathway, is transferred via mossy fibers to the CA3 region, and then via Schaffer collaterals to the major hippocampal output structure, the CA1, which in turn mainly projects back to the entorhinal cortex either directly or via the subiculum (van Strien et al., 2009). Neurotransmitters play a central role in this circuit and trafficking of their receptors is involved in the synaptic plasticity which mediates memory consolidation, i.e., the transfer of information from short-term to long-term memory (Collingridge et al., 2004; Groc and Choquet, 2020; Malinow and Malenka, 2002; Zhong et al., 2020).

Previous studies have provided detailed insights into the regional and laminar distribution patterns of multiple neurotransmitter receptors in the human hippocampal regions (Biegon et al., 1982; Palomero-Gallagher et al., 2020; Perry et al., 1993; Szot et al., 2005; Tremblay et al., 1985). The hippocampal expression patterns of genes coding for these neurotransmitter receptors or for their subunits have also been described (Hawrylycz et al., 2015, 2012; Szot et al., 2005). Furthermore, Vogel et al. (2020) performed a transcriptome-wide screening along the longitudinal axis of the human hippocampus by using human gene expression data and macroanatomical labels from the Allen Human Brain Atlas (Hawrylycz et al., 2012), and found a regionally specific anterioventral-posteriodorsal gradient of gene expression profiles. However, no studies have systematically and comprehensively analyzed the relationship between the densities of multiple classical neurotransmitter receptors and the expression levels of their encoding genes in the hippocampus. Since many neurologic and neuropsychiatric disorders such as epilepsy and Alzheimer's disease are associated with both a genetic predisposition and an altered balance in the densities of multiple receptors (Graebenitz et al., 2011; Khan et al., 2021; Palomero-Gallagher et al., 2012; Selkoe, 2001; Symonds et al., 2017), elucidating the relationship between gene expression levels and receptor densities could deepen our understanding of the pathogenesis of such diseases, and provide insights into the specific link between disease-associated genes and the disease itself.

Specific cyto- and receptor architecture as well as gene expression patterns have been related to differences in cortical function (Amunts and Zilles, 2015; Burt et al., 2018; Zilles and Palomero-Gallagher, 2017). Thus, our study aimed to simultaneously quantify the densities of 14 neurotransmitter receptors and the expression levels of their 43 encoding genes separately for the DG and CA hippocampal regions in tissue from the same brain samples, and then map the relationships between the ensuing receptor densities and expression levels of the corresponding genes.

2. Materials and methods

2.1. Tissue collection and processing

We obtained six hippocampus samples from the Netherlands Brain Bank in accordance with ethical and legal declarations (Kliouevа et al., 2018) and one sample through the body donor program in compliance with the Ethics Committee of the Department of Anatomy, University of Düsseldorf, Germany. All donors (71 ± 15 years of age; 5 females; 2 males; European origin) did not have a history of neurologic or psychiatric disease, and the postmortem delay of autopsy (postmortem interval) was less than 5 h.

Since chemical fixation alters the physiological properties of receptor subunits, it affects the specific and nonspecific receptor binding, and consequently results in density measurements that do not reflect the true receptor concentrations (Palomero-Gallagher and Zilles, 2018; Zilles et al., 2002). Therefore, unfixed brain tissue was shock-frozen in isopentane at −40 °C immediately after autopsy and stored until further processing in air-tight plastic bags at −80 °C to protect it from freeze-artifacts.

After quality control by visual examination, the hippocampus samples were serially sectioned coronally by means of a cryostat microtome (Leica CM3050 S) at around −20 °C. For each subject's sample, the first three series of 20 µm sections, each comprising a total of 20 sections, were collected for receptor autoradiography and cell-body staining. Then, 10 sections, each 60 µm thick, were obtained for RNA isolation and quantification (Supplementary Fig. S1). Finally, three further series of 20 µm sections, also comprising a total of 20 sections each, were collected for receptor autoradiography and cell-body staining. Each section destined to the visualization of receptor or cell body distribution patterns was thaw-mounted onto a pre-cooled, silanized glass slide upon sectioning, then air dried and stored in air-tight plastic bags at −80 °C until further processing. For each section collected for analysis of RNA expression, the CA and DG regions were dissected inside the cryotome with a scalpel upon sectioning, then each region (CA/DG) was separately transferred to a tube filled with QIAzol Lysis Reagent (Qiagen, Hilden, Germany) and stored at −80 °C until further RNA extraction in one batch to ensure the same experimental conditions for all samples.

2.2. *Quantitative* in vitro *receptor autoradiography*

Alternating sections were processed for visualization and quantification of 14 different neurotransmitter receptor binding sites by means of quantitative *in vitro* receptor autoradiography according to previously published protocols and quality controls (Palomero-Gallagher and Zilles, 2018; Zilles et al., 2002), or for the visualization of cell bodies by means of a modified silver cell body staining procedure (Merker, 1983). All sections collected for the visualization of cell bodies or of a given receptor type were processed together. Thus, within a given modality, we could ensure the same experimental conditions for all samples. Histologically processed sections served to confirm the delineation of the CA and DG regions in the receptor autoradiographs. Supplementary Table S1 provides a list of the analyzed receptors together with their classification based on type and mechanism of action, as well as the corresponding binding protocols.

The receptor binding procedure encompassed a preincubation step to rehydrate sections, a main incubation step with a tritiated ligand known to bind specifically to one of the targeted receptor types, and a washing step to rinse off residual tritiated ligand. For each targeted receptor type and in parallel with the main incubation to detect the total binding of each tritiated ligand, which was carried out with five sections per sample, an additional section per sample was incubated with the tritiated ligand plus a non-labeled specific displacer to determine the proportion of the non-displaceable (i.e., non-specific) binding. Specific binding is the difference between total and non-specific binding. However, since non-specific binding was found to be less than 5% of the total binding sites (see below for details), the latter was defined here as specific binding.

The radioactively labeled sections were exposed against tritium-sensitive films together with plastic standards of known concentrations of radioactivity for 9 to 15 weeks (Supplementary Table S1) and the ensuing autoradiographs were digitized with a CCD camera and processed densitometrically for the analysis of receptor densities (Palomero-Gallagher and Zilles, 2018; Zilles et al., 2002). In short, transformation curves, calculated based on the plastic standards, were used to indicate the relationship between gray values in the autoradiographs and receptor densities (fmol/mg protein) in the tissue (Palomero-Gallagher and Zilles, 2018; Zilles et al., 2002). Images were subsequently linearized by means of the transformation curves. For visualization purposes, these linearized images were smoothed, contrast enhanced, and pseudo-color coded in a spectral order to optimize visualization of regional and laminar receptor distribution patterns. Finally, the in-house-developed software AnaRec (Impieri et al., 2019) was used to quantify the receptor densities in architectonically identified hippocampal CA and DG regions in both the sections processed for visualization of total binding sites and those for identification of non-specific binding. Depending on section quality (e.g., presence of technically related artifacts such as tears or folds), total binding was quantified in 3–5 sec-

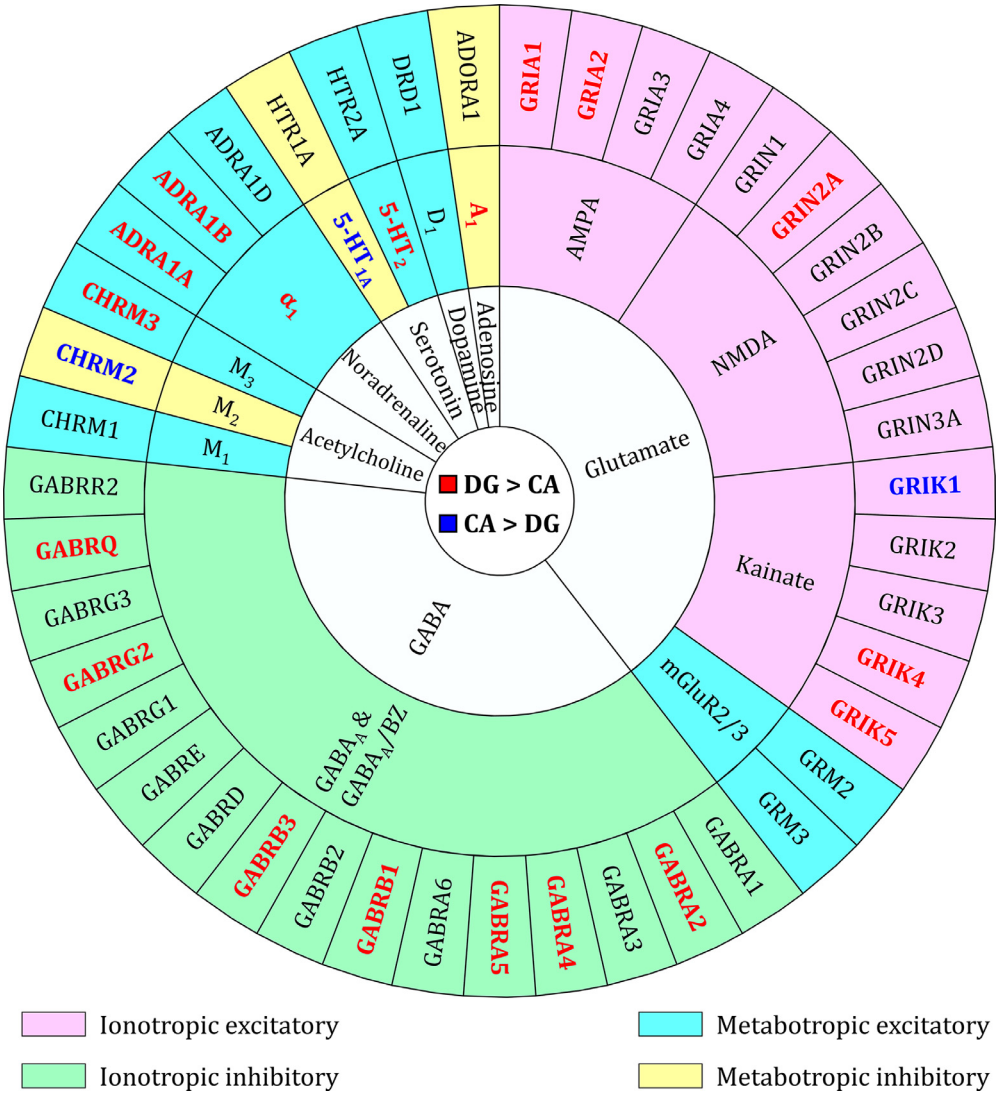

Fig. 2. Neurotransmitter receptors and their corresponding genes. Comprehensive list of the neurotransmitter receptors and their corresponding genes analyzed in the present study. Colors have been used not only to differentiate receptors by their effect (excitatory or inhibitory) and mechanisms of action (ionotropic or metabotropic), but also to highlight the significant results of our statistical analyses. Names highlighted in red or blue indicate significant differences in receptor densities or gene expression levels between the CA and DG regions after partial Bonferroni correction (Scholtens et al., 2014). Further information is provided in Supplementary Tables S3 and S4.

tions per receptor type and sample. The mean densities of all 14 receptors were visualized for the DG and CA separately in a polar-coordinate plot, and the resulting graph constitutes the "receptor fingerprint" of the region in question (Zilles et al., 2002).

Based on their mechanisms of action, neurotransmitter receptors are classified into ionotropic and metabotropic receptors (Hall and Hall, 2020). Ionotropic receptors consist of different subunits, and each subunit is encoded by a single gene, so that an ionotropic receptor is jointly encoded by a composition of multiple genes (Fig. 1). Conversely, metabotropic receptors are monomeric structures and thus only encoded by one gene, which were further selected to perform across-gene correlation analysis. Of the receptor types analyzed here, AMPA, NMDA, kainate, $GABA_A$, and $GABA_A$/BZ are ionotropic receptors, whereas mGluR2/3, M_1, M_2, M_3, α_1, 5-HT_{1A}, 5-HT_2, D_1 and A_1 are metabotropic receptors (Supplementary Table S1). However, since the ligands used to label the mGluR2/3 and the α_1 receptors are subtype non-specific antagonists, it was necessary to analyze all encoding genes in parallel for these two metabotropic receptors. Fig. 2 provides an overview of the neurotransmitter receptors analyzed in the present study and their corresponding genes.

2.3. RNA isolation and quantification

The processing of tissue and RNA was done by the same experimenter in one batch for all samples at the core NGS Core Facility of the University of Bonn, Germany. For each of the subjects, tissue samples from the CA or DG regions were placed in different tubes filled with QIAzol solution to lyse the tissue and protect the isolated RNA from degradation. All subsequent steps were performed simultaneously for all probes, to ensure the same experimental conditions for all samples. Then, each lysate was resuspended with a filter-tipped pipette to dissolve remaining fragments. Subsequently, the samples were aliquoted into portions reflecting about 20 mg tissue and stored at −80 °C until isolation. Finally, total RNA was isolated using the Qiagen miRNeasy Micro Kit (Qiagen, Hilden, Germany) according to the manufacturer instructions.

Quality control of total RNA was performed using a TapeStation (Agilent, Santa Clara, USA). Libraries for sequencing were prepared using the QuantSeq 3′mRNA-Seq Library Prep Kit FWD for Illumina (Lexogen, Vienna, Austria) in accordance with manufacturer instructions. Reads were sequenced on a HiSeq 2500 V4 (Illumina, San Diego, USA). Approximately 16 million single-reads of 100 bp length were obtained per sample library.

The quantification of RNA samples was performed using the Lexogen QuantSeq pipeline implemented in the Partek® Flow® Genomic Analysis Software, with small modifications. Briefly, trimmed reads were aligned to the hg38.p13 reference index using STAR - 2.7.3a (deviation from default settings: filtering BySJout; max. read mapping 20; max. mismatches 999; mismatch mapped ratio 0.1; min. intron size 20; min. spliced alignment overhang 8; min. annotated spliced alignment overhang 1). Aligned reads were quantified using Partek E/M against

hg38.p13 - Ensembl Transcript release 103. Read counts for each gene were normalized to counts per million (CPM). One DG sample was identified as an outlier in principal component analysis and excluded from further analysis (Supplementary Fig. S2). For differential gene expression analysis, gene counts were normalized using trimmed mean of M values (TMM) (Robinson and Oshlack, 2010).

Based on information provided by the human gene database (https://www.genenames.org/), 47 receptor encoding genes were identified and selected for further analysis. During quality control of RNA-Seq data, four genes (*GRIN3B, GABRP, GABRR1*, and *GABRR3*) were excluded for further analyses (Fig. 2). The mean expression levels of the 43 analyzed receptor encoding genes were visualized for the DG and CA separately in the form of a polar-coordinate plot. Analogous to the receptor fingerprint, this resulting graph provides a region-specific expression profile of multiple genes, i.e., the "RNA fingerprint" of the area in question.

2.4. Statistical analysis of receptor densities and gene expression levels

Differences in receptor densities and gene expression levels between CA and DG were analyzed with a non-parametric permutation test (10,000 permutations) (Nichols and Holmes, 2002). A partial Bonferroni correction method was used to control for multiple comparisons in a relatively conservative way, while still keeping enough sensitivity (Scholtens et al., 2014). Specifically, the receptor densities (fmol/mg) and normalized RNA counts were separately used for decomposing and processing with principal component analyses (PCA), the four first principal components together were found to explain 95% of receptor and corresponding gene data, respectively (Supplementary Table S2). Thus, the p value threshold of multiple comparisons correction for each data was set at 0.0125 (0.05/4). Unless otherwise specified, only corrected p values are described in the results section. To ensure the replicability and robustness of the above analyses, a leave-one-observation-out cross-validation (LOOO–CV) approach (Schurger et al., 2010) was performed by repeating the analyses while one observation data was removed from the corresponding dataset at a time to determine if the result would remain significantly different. Furthermore, the effect size and statistical power were also calculated (Charan and Kantharia, 2013; Cohen, 1992).

In addition, for further comparison of the variability of RNA expressions in hippocampal regions from different subject sample, the RNA expression differences between CA and DG were analyzed using data obtained from the Allen Human Brain Atlas (Hawrylycz et al., 2015, 2012). We used the JuGEx tool, which integrates RNA expression data in the Allen Human Brain Atlas with cytoarchitectonic probability maps from the Julich-Brain Atlas (Amunts et al., 2020) to extract the necessary data (Bludau et al., 2018). A detailed description of this procedure was published in Bludau et al. (2018), and summarized here in the section Supplementary Material and Methods.

The relationship between the density of each receptor type and the expression level of the corresponding gene or subunit gene was analyzed across subjects (within-gene correlation analysis) with a Spearman rank correlation (r), which is more robust to outliers than Pearson's correlation (Schober et al., 2018). Specifically, 7 data points, each representing one of the analyzed samples, were used for calculating the correlation in CA, however 6 data points were used in DG as one DG sample had been identified as an outlier in RNA isolation and quantification and excluded from further analysis. The r value threshold of moderate strength of the correlation was set at 0.4/−0.4 (Schober et al., 2018), and the p value threshold of multiple correction was also set at 0.0125. In addition, the mean correlation coefficients were calculated based on the different conditions, e.g., mean correlation strength in the entire hippocampus, the CA, or the DG, respectively. For cross-validating the correlation coefficient (r), the LOOO–CV method was conducted by repeating the correlation analysis while one subject data was removed at a time, and then the mean correlation coefficient ($r_{\text{Looo-cv}}$) was calculated. Furthermore, we performed an across-gene correlation analysis with the partial metabotropic receptors and their corresponding genes separately in the CA and DG regions, and the detailed information was provided in Supplementary Fig. S3.

In addition, the Spearman correlation coefficient was used as a distance parameter in a multidimensional scaling analysis (MDS) (Cox and Cox, 2008) to map the relationship pattern of the ionotropic receptors and their corresponding subunit genes.

3. Results

3.1. CA and DG differ in their receptor and RNA fingerprints

In the human hippocampus, the analyzed receptors present distinct regional and laminar distribution patterns (Fig. 3). The densities of AMPA, mGluR2/3, $GABA_A$/BZ, α_1, and 5-HT_2 receptors are higher in DG than in CA, and the opposite holds true for the NMDA, $GABA_A$, 5-HT_{1A}, and A_1 receptors, thus resulting in receptor fingerprints of comparable sizes, but very different shapes for the CA and DG regions (Fig. 4A). However, only the differences in α_1, 5-HT_{1A}, 5-HT_2, and A_1 metabotropic receptor densities were statistically significant and confirmed by the validation analysis (Fig. 2 and Supplementary Table S3). Within CA, the CA1 region presents the highest densities of most of the analyzed receptors, with the notable exception of the kainate, α_1, and 5-HT_2 receptors, which are present at higher concentrations in CA3 than in CA1 (Fig. 3).

In contrast to the situation described for the receptor fingerprints, the corresponding RNA fingerprints of the CA and DG regions differ in size, but are similar in shape, indicating that both hippocampal regions differ in their absolute gene expression levels, but not in the balance in the expression levels of the analyzed genes (Fig. 4B). The DG presents significantly higher *GRIA1* and *GRIA2* (for the AMPA receptor); *GRIN2A* (NMDA); *GRIK4* and *GRIK5* (kainate); *GABRA2, GABRA4, GABRA5, GABRB1, GABRB3, GABRG2*, and *GABRQ* ($GABA_A$ and $GABA_A$/BZ); *CHRM3* (M_3); as well as *ADRA1A* and *ADRA1B* (α_1) expression levels than does CA (Fig. 2 and Supplementary Table S4). Significantly lower gene expression levels in DG than in CA were found only for the kainate encoding gene *GRIK1* and the M_2 encoding gene *CHRM2*. Thus, we identified 17 genes showing significantly different expression levels between CA and DG regions. The results of the validation analysis underline the reproducibility of these statistical findings concerning region-specific differences (Supplementary Table S4). In addition, *GABRA6, GABRE*, and *GABRR2* present extremely low gene expression levels (Supplementary Table S4), thus they were excluded in the further relationship analyses between receptors and corresponding genes. Interestingly, a comparable analysis using the edited Julich-Brain maps to precisely select independent RNA data from the Allen Human Brain Atlas only revealed a few significantly higher gene expression levels in DG than in CA, and no significantly lower gene expression levels were found in DG than in CA (Supplementary Table S5). Specifically, we only found the expression levels of *GRIA4, GRIK2, GRM2, GABRB3*, and *ADRA1A* to be significantly higher in DG than in CA (Supplementary Table S5).

Of particular interest is the fact that significant differences in receptor densities were found only for metabotropic receptors, but significances in encoding gene expressions mostly pertained to ionotropic receptors. Furthermore, only the α_1 receptor shows both significantly higher receptor densities and encoding gene expression levels in DG than in CA. Interestingly, although 5-HT_{1A}, 5-HT_2, and A_1 receptor densities in CA and DG differed significantly from each other, no significances were found for the expression levels of their different encoding genes (Fig. 2 and Supplementary Tables S3 and S4). Taken together, these results point at a poor covariation expression phenomenon between encoding genes and corresponding receptors in the hippocampus, i.e., for most of the receptors analyzed here differences in their densities between the CA and DG regions do not match the differences between these regions in the expression levels of the corresponding genes.

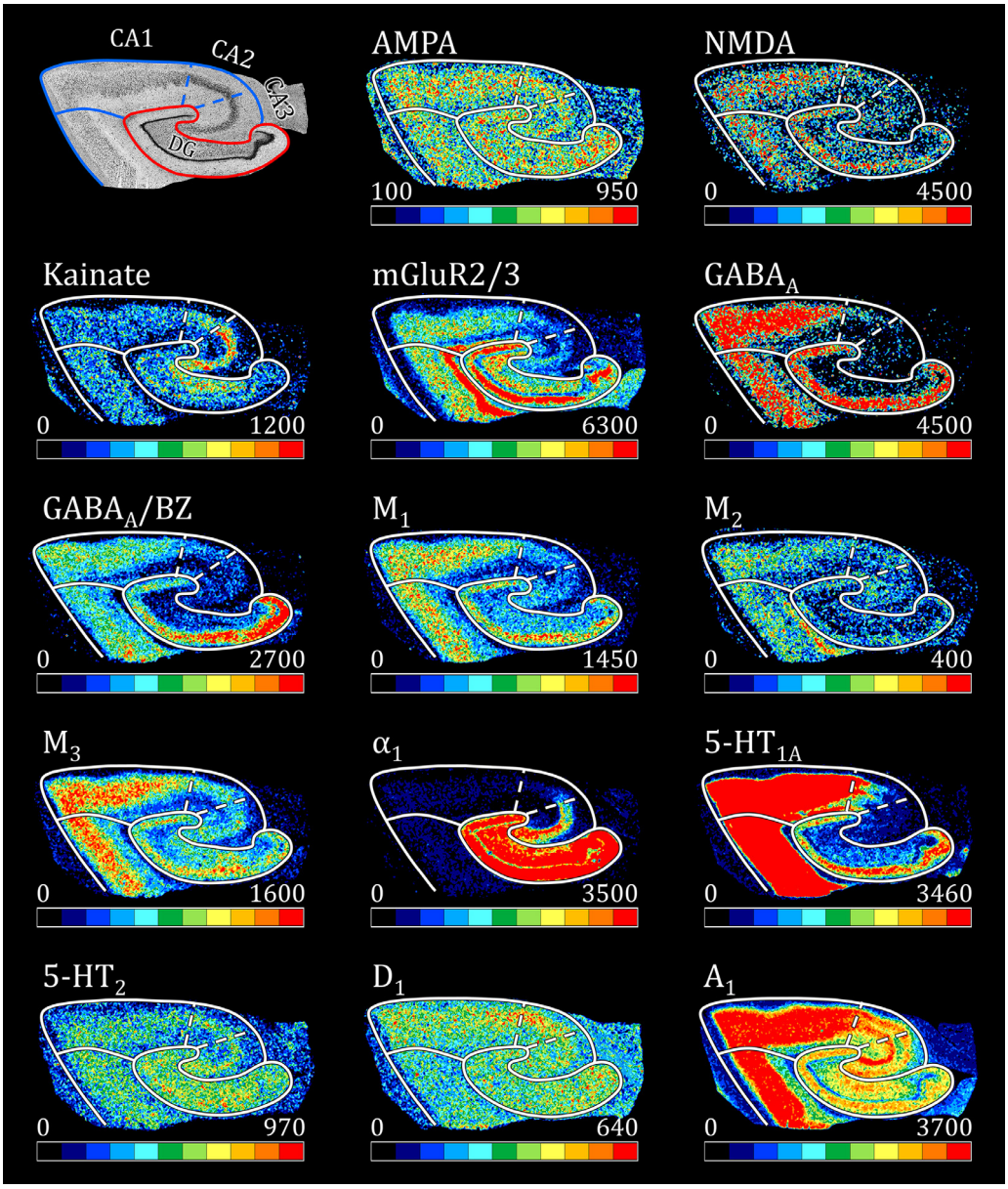

Fig. 3. Regional and laminar distribution patterns of cell bodies (cytoarchitecture) and of neurotransmitter receptors (receptor architecture) in the human hippocampus. The CA1-CA3 subregions of CA are delineated with dashed lines. Color scales code for receptor densities in fmol/mg protein. Abbreviations: CA1-CA3, regions 1–3 of *Cornu Ammonis*; and DG, dentate gyrus.

3.2. Correlations between receptor densities and encoding gene expression levels

For the within-gene correlation analysis, the correlation coefficients between receptors and their corresponding genes vary widely from negative to positive, with −0.8286 and 0.9286 being the extreme values (Supplementary Table S6). The results of the LOOO–CV present a high similarity with the above described statistical findings, which further prove their reproducibility and robustness (Supplementary Table S6). However, the mean correlation coefficients are poor for CA (0.09) and DG (0.20). Furthermore, we computed this measure for the entire hippocampus, which yielded a value of 0.15. Considering some receptors with many subunits or subtype may weigh heavily the calculation of the mean correlations, we provide two alternative strategy for cross verification. (1) Assigning each receptor with the mean correlation by averaging the correlation coefficients between receptor density and its main subunit genes (Supplementary Tables S6 and S7), the mean correlation coefficients are 0.16 for CA, 0.11 for DG, and 0.14 for hippocampal formation. (2) Averaging the main subunit gene expressions for a given receptor type for each subject before running the within-gene correlation analysis, the mean correlation coefficients are 0.15 for CA, 0.12 for DG, and 0.14 for hippocampal formation; we further found a poor congruent receptor-gene alignment between CA and DG (Supplementary Fig. S3A and Table S8). Taken together, these results indicate that the mean correlation coefficients for the entire hippocampal formation ranging from 0.14 to 0.15 represent the high reliability. In contrast, the results of the across-gene correlation analysis with the partial metabotropic receptors and their corresponding genes reveal a high correlation in both CA (0.57) and DG (0.71) (Supplementary Fig. S3B). Moreover, we averaged main subunit gene expressions of all subjects to a receptor, then analyzed across-gene correlation analysis with the 14 receptors and found a high robustness results in both CA (0.60) and DG (0.64).

After filtering the moderate-to-strong correlation strength (0.4–1.0) between receptors and their respective encoding genes revealed by the

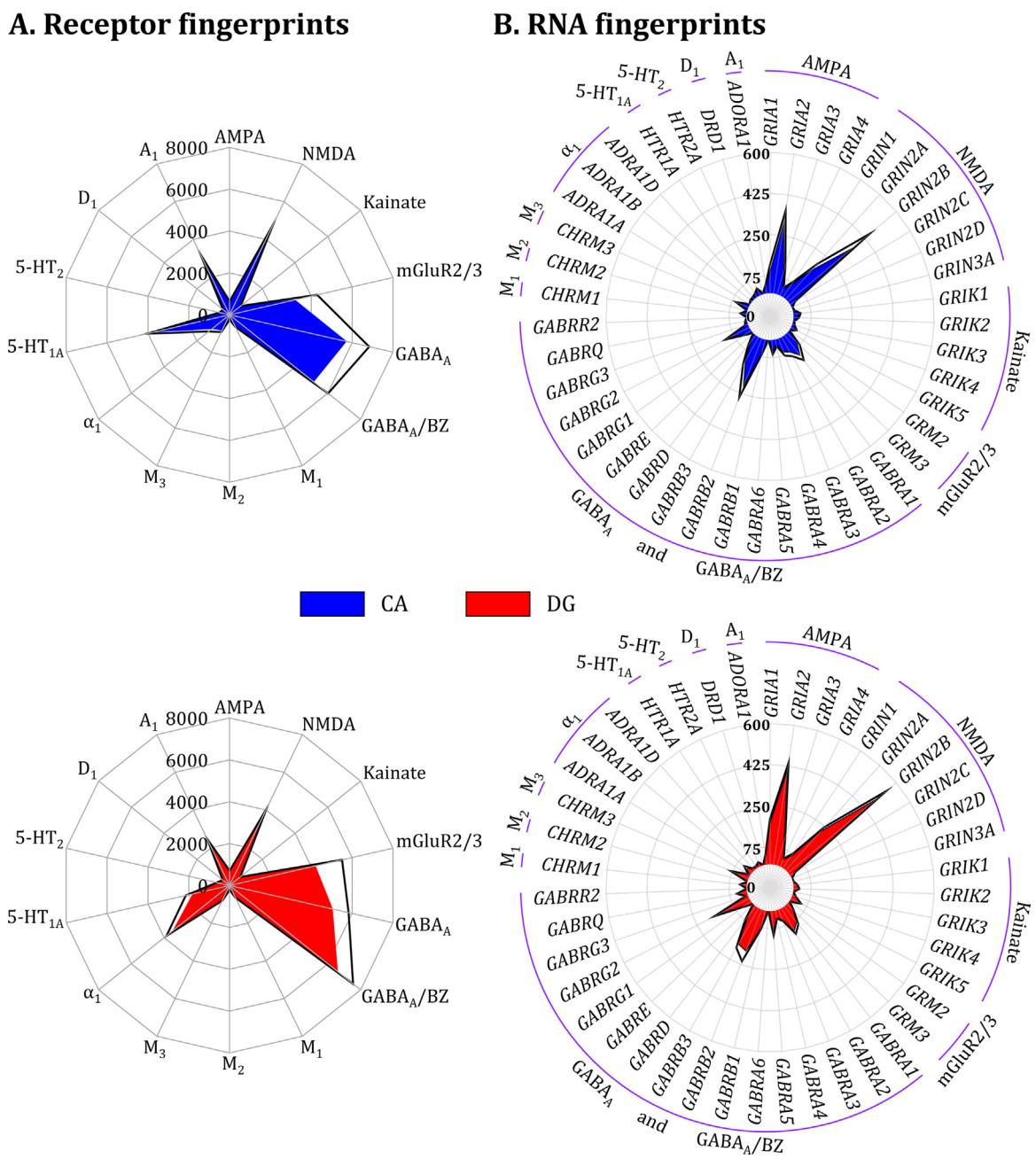

Fig. 4. Fingerprints of receptor and corresponding gene in the human hippocampus. (A) Receptor fingerprints depict the mean densities (thick black line indicates the standard deviation) of all 14 analyzed receptors in the CA and DG regions. (B) Corresponding RNA fingerprints depict the mean expression levels (thick black line indicates the standard deviation) of all 43 analyzed genes in the CA and DG regions. Note, to facilitate visualization of low RNA counts, we have expanded the scale range. The order of receptor and corresponding gene types is identical with Fig. 2. The underlying data are provided in Supplementary Tables S3 and S4, and made freely available to the neuroscientific community via the EBRAINS platform (DOI to be released upon publication).

within-gene correlation analysis, the CA and DG regions display differential patterns both in positive and negative correlations (Fig. 5). Specifically, the DG region presented a higher number of high-strength correlations with corresponding receptors than did the CA region (24 vs. 15 genes, respectively, out of the 43 genes analyzed) (Supplementary Table S9). Interestingly, there was an overlap between the genes showing high-strength correlations and the genes which were found to be expressed at significantly different levels in the CA and in the DG regions, whereby the ratio of overlapping genes was larger for CA (10/15) than for DG (9/24) (Supplementary Fig. S4).

For the moderate-to-strong correlation strength, the only positive correlations present in both CA and DG are those of NMDA with *GRIN1*, mGluR2/3 with *GRM3*, and $GABA_A$ with *GABRG2* (Fig. 5). In addition, CA and DG show no common correlation patterns concerning the negative correlation coefficients (Fig. 5). Interestingly, we found a higher number of correlations between receptors and their encoding genes in DG than in CA. Furthermore, in the CA region we mainly found high-strength correlations between ionotropic receptors and their encoding genes (Fig. 5A), whereas in the DG we also found high-strength positive and negative correlations for multiple metabotropic receptors (Fig. 5B). Finally, in CA we found more positive high-strength correlation coefficients for the $GABA_A$ receptor than for the $GABA_A$/BZ binding site, and the opposite holds true for the DG region (Fig. 5), although these two binding sites for GABA share the same encoding genes.

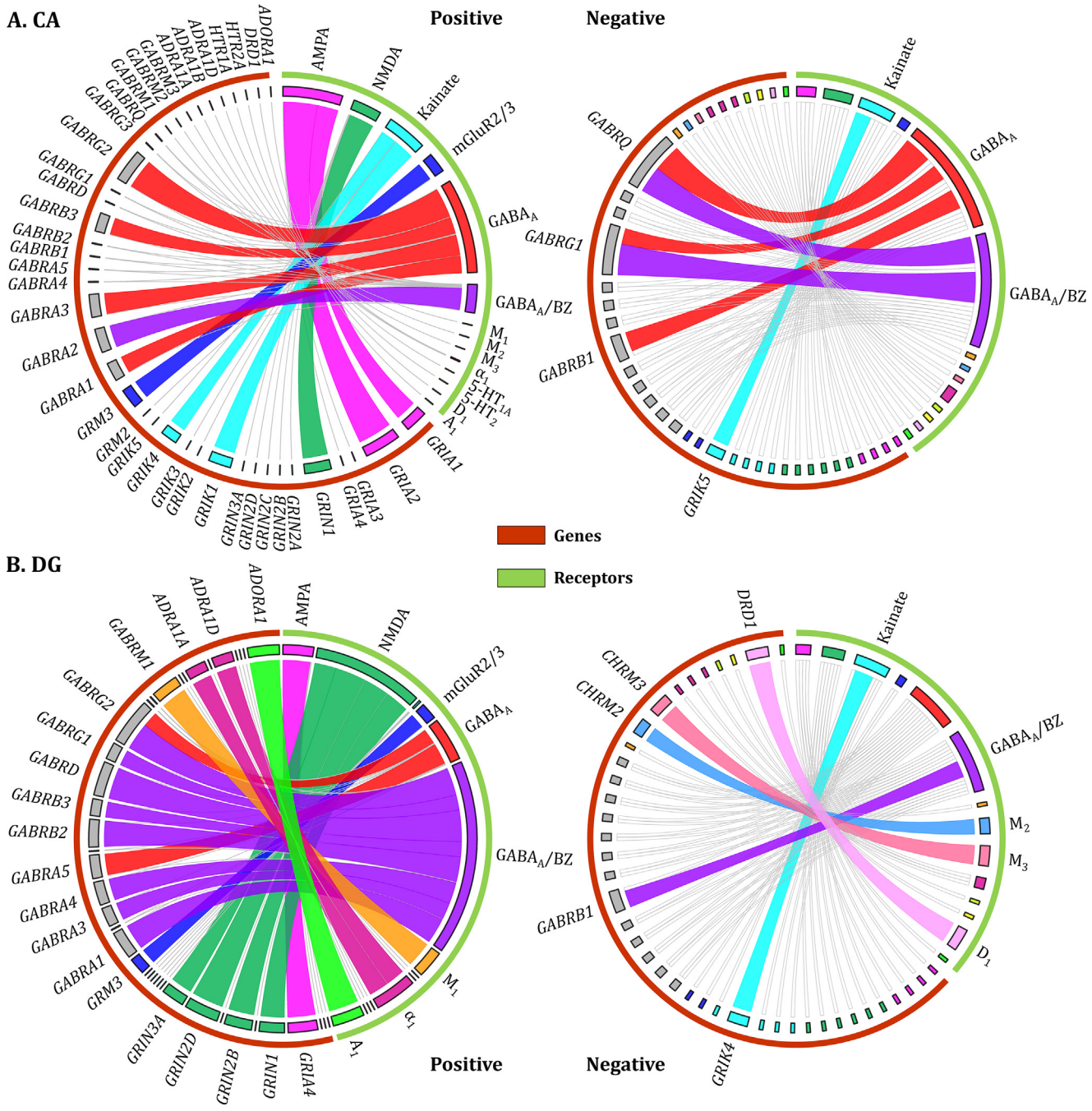

Fig. 5. Correlation patterns of receptor densities and corresponding gene expression levels in the human hippocampus. (A) Correlations in the CA region. (B) Correlations in the DG region. For both regions the positive correlations are shown in the left plot and negative ones in the right plot. The ribbons show the correlation coefficient at moderate-to-strong strength (0.4–1.0), while the gray lines indicate the correlation coefficient at weak strengths (0.0–0.4). Further information concerning correlation coefficients is provided in Supplementary Table S6.

3.3. Multidimensional scaling analysis

The correlation coefficients between genes and corresponding receptors were found to be significant in the case of the AMPA receptor with *GRIA2* and $GABA_A$ with *GABRG2* in the CA region, as well as for NMDA with *GRIN2D* and $GABA_A$/BZ with *GABRD* in the DG region (Supplementary Table S6). However, only the correlation coefficient between the AMPA receptor and *GRIA2* in CA remains significant after partial Bonferroni correction (Fig. 6A). Interestingly, the MDS revealed opposing relationships between the AMPA receptor and its encoding subunit genes in the CA and DG regions, since in CA *GRIA2* presented the strongest and *GRIA4* the weakest correlation coefficients with AMPA, whereas the opposite holds true for DG (Fig. 6B).

4. Discussion

We analyzed the regional densities of 14 neurotransmitter receptors and expression levels of their corresponding 43 encoding genes in the CA and DG hippocampal regions from the same brain samples. Neurotransmitter receptor densities presented distinct regional and laminar distribution patterns, and the CA and DG also differed in their gene expression levels. Significant differences in receptor densities between CA and DG were found only for metabotropic receptors, but in encoding

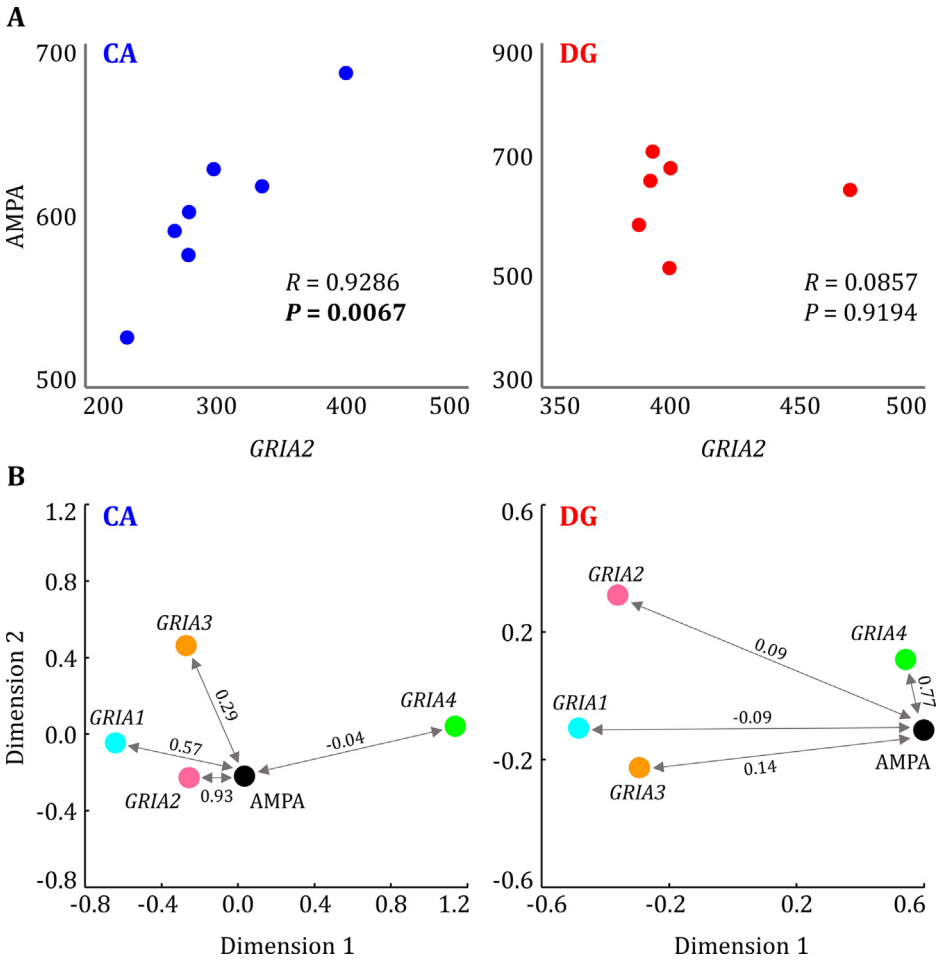

Fig. 6. Relationships between the AMPA receptor and corresponding genes in the human hippocampus. (A) Significant correlation coefficient between AMPA receptor density and *GRIA2* expression level in CA but not in DG. Plots depicting the relationships between all other analyzed receptors and their corresponding genes are provided in Supplementary Fig. S5. (B) Multidimensional analyses (MDS), based on the Spearman rank correlation coefficients between the AMPA receptor and its corresponding subunit genes, reveal opposite distribution patterns of relationships in CA and DG regions. Further information concerning MDS between other analyzed receptors and their corresponding subunit genes is provided in Supplementary Fig. S6.

gene expressions mostly for ionotropic receptors. Furthermore, the receptor fingerprints of the CA and DG regions differ in shape but have a similar size, however the opposite holds true for the RNA fingerprints. These results provide evidence that expression levels of encoding genes and densities of the corresponding receptors do not covariate, which was further characterized by their correlation analyses. The correlation coefficients between receptors and their encoding genes vary widely in strength, and the mean correlation coefficient only presents a weak strength. It is worth noting that a significant correlation was found only for AMPA and *GRIA2* in the CA region, and the relationships between the AMPA receptor and its corresponding subunit genes display diametrically opposite trends in CA and DG.

Functional differentiation of the cortex has been correlated with specific regional differences in cytoarchitecture, receptor architecture and gene expression levels (Amunts and Zilles, 2015; Burt et al., 2018; Hawrylycz et al., 2015, 2012; Zilles and Palomero-Gallagher, 2017). The distinctive regional and laminar receptor distribution patterns of hippocampal regions in the present study are in accordance with our previous research (Palomero-Gallagher et al., 2020), however to the best of our knowledge this is the first report of differential expression levels of corresponding receptor-encoding genes in the CA and DG regions from the same brain. The densities of the 14 analyzed receptor types and the expression levels of the 43 corresponding genes were visualized for each region as its receptor fingerprint and RNA fingerprint, respectively. Fingerprints depict the region-specific balance of multi-receptor densities or gene expressions and thus reveal the locally specific neurochemical or transcriptional organization at the receptor or gene level, respectively. Interestingly, receptor fingerprints of the CA and DG regions differ in shape but have a similar size, but the opposite holds true for the RNA fingerprints. Thus, CA and DG regions present a comparable balance in the expression levels of the analyzed genes, but not in the densities of the receptors they encode. These differences suggest a poor covariation between genes expression levels and receptor densities in the CA and DG regions, which was further verified by the correlation analyses.

This poor covariation phenomenon could be partially explained by the complex gene-encoding-receptor expression mechanisms (Levitz et al., 2016; Payne, 2015; Schwappach, 2008; Stephenson et al., 2008), which can result in nuanced relationships between different receptor types and their encoding genes. The complexities of regulation mechanisms are governed by gene transcription, translation, proper protein folding and co-assembly in the endoplasmic reticulum, post-translational modifications, and subsequent trafficking to the target membrane surface along the secretory pathway (Fig. 1), as well as by remarkably different degradation rates for mRNA (minutes) and protein/receptor (hours to years) and different tissue situation between postmortem and alive (Buccitelli and Selbach, 2020; Payne, 2015). The complexity of biological regulation mechanisms seems to make the relationship between receptors and corresponding genes unpredictable (Buccitelli and Selbach, 2020; Payne, 2015). In accordance with this assumption, our results strongly suggest that in the human hippocampus region-specific receptor densities cannot simply be derived from the expression levels of corresponding genes, as reflected by their widely varying correlation coefficients. Furthermore, the mean correlation coefficient for the entire hippocampus (r=0.36) based on within-gene correlation analysis is weak and consistent with the correlation coefficients between genes and proteins reported in previous studies (Battle et al., 2015; Gry et al., 2009; Vogel et al., 2010; Zhang et al., 2014). In contrast, the across-gene correlation

analyses display relatively high correlations in CA (r=0.57) and DG (r=0.71), which further provide evidence for the fact that across-gene correlations are generally higher than within-gene correlations as the variation between genes largely exceeds the variation within genes (Buccitelli and Selbach, 2020; Fortelny et al., 2017). It is worth noting that only one previous study performed across-gene correlation analysis between mRNA and protein expression levels in human brain tissue, and described a moderate correlation (r=0.54, r^2 = 0.29) (Wang et al., 2019). This relatively low r^2 value means that the variability in mRNA levels explains less than 30% of the variability in protein levels in human brain tissue (Wang et al., 2019). This is in agreement with previous studies (de Sousa Abreu et al., 2009; Schwanhäusser et al., 2011; Vogel et al., 2010; Vogel and Marcotte, 2012), which demonstrated that around 40% of the variation in protein concentration may be explained by knowing mRNA abundances by using mammalian cell lines. Multiple post-transcriptional, translational, and protein degradation regulations play critical roles in contributing to explain the remaining more than 60% of the variation (Buccitelli and Selbach, 2020; Liu et al., 2016; Schwanhäusser et al., 2011; Vogel et al., 2010; Vogel and Marcotte, 2012). The relatively low explanatory power (2%) in the present study not only arises from the fact that we performed a within-gene correlation analysis, which generally yields lower values than across-gene analyses (Buccitelli and Selbach, 2020), but also from the important fact that mechanisms governing receptor expression are even more complex than those of proteins, since they additionally involve, e.g. receptor assembly and trafficking steps (Levitz et al., 2016; Schwappach, 2008; Stephenson et al., 2008). Taken together, gene expression levels in the CA and DG regions cannot be directly used as proxies for receptor densities in the respective hippocampal regions.

Interestingly, the range of correlation coefficients between receptors and their corresponding genes varied widely depending on the combination of receptor type and hippocampal region. Furthermore, the genes presenting moderate-to-strong correlations with corresponding receptors in CA have a striking overlap with the genes which display significantly different expression levels when comparing CA with DG. Importantly, we also demonstrated a differential pattern of high-strength correlation between receptor densities and expression levels of their respective encoding genes in the CA and DG regions. This different expression pattern between CA and DG regions may closely associate with their respectively specific principal cell types, physiological properties, and regional functional differentiation. The DG region, with its cellular layer consisting of granule cells, is the primary gateway of the trisynaptic loop, and plays a crucial role in code transformation between cortical afferents and the hippocampus, as well as in pattern separation (Acsády and Káli, 2007; Dieni et al., 2016). The CA region, with its pyramidal cell layer, possesses an unusual autoassociative memory network in the CA3 region and displays extensive interconnectivity among the CA3, CA2, and CA1 regions, which is critical for short-term and long-term potentiation (Acsády and Káli, 2007). Its unique synaptic plasticity underlying learning and memory occurs dynamically in the CA and DG regions, which necessarily requires the high participation of specific receptor trafficking (Collingridge et al., 2004; Groc and Choquet, 2020; Malinow and Malenka, 2002). Therefore, the different high-correlation patterns in CA and DG may imply that the receptor expression mechanisms are not only controlled by genetic information, but also associated with specific physiological properties of different cell types as well as with modifications of regional functional differentiation.

Concerning the AMPA receptor and its corresponding subunit genes, the hippocampus is enriched with GluA1, GluA2, and GluA3 receptor subunit expression, while it has a lower GluA4 expression (Yadav et al., 2017). This is in agreement with the expression levels we demonstrated here for the corresponding genes. Interestingly, the AMPA receptor and its corresponding subunit genes present completely opposite distribution patterns in the CA and DG regions. It is worth noting that there is a significant positive correlation between the AMPA receptor density with *GRIA2* subunit gene expression level in the CA region. Previous studies have demonstrated that the pyramidal cells of the CA region express AMPA receptors predominantly composed of the GluA2 subunit, which is encoded by *GRIA2*, in complex with either GluA1 or GluA3 subunits (Greger et al., 2017; Haselmann et al., 2018). In addition, the GluA2 subunit regulates the critical biophysical properties of the AMPA receptor, strongly impacts receptor assembly and trafficking, and plays critical roles in synaptic transmission and long-term synaptic plasticity (Greger et al., 2017; Haselmann et al., 2018; Isaac et al., 2007). Thus, the expressions of GluA2 and encoding gene *GRIA2* can be selectively changed in response to specific pattern stimuli at different regional synapses (Haselmann et al., 2018; Yadav et al., 2017). These findings further indicate that the relationships between gene expression levels and receptor densities are mediated and modified by multiple post-translational specific-regional factors (Battle et al., 2015).

Surprisingly, we observed some differences in gene expression levels between data obtained from our brain samples and data derived from the Allen Brain. This could be explained in part by the fact that different approaches were used to obtain the tissue/cell samples for RNA extraction, which resulted in the analysis of different cellular populations. Samples from the Allen Brain were obtained by “laser ablation” specifically from the granular layer of the DG and from the pyramidal layer of the CA region. Thus, these samples contained the cell bodies of the main neuronal types of these two regions, i.e., of granular and pyramidal cells, respectively. In contrast, we obtained our RNA expression levels from homogenates of the DG and CA regions. The DG homogenate encompassed the molecular, granular, and polymorph layers of the fascia dentata, as well as the CA4 region, while the CA homogenate contained the oriens, pyramidal, radiatum and lacunosum-molecular layers of the CA1-CA3 regions and the lucidum layer of CA3. Since the overall cellular organization of the DG and CA regions is more complex than hitherto thought and hippocampal layers differ in their cellular composition (Yao et al., 2021), each of these homogenates not only contained cell bodies of the principal neuronal type of each region, but also those of other cell types such as the radiatum giant cells or ivy cells in the radiatum layer (Gulyás et al., 1998; Somogyi et al., 2012), the neurogliaform, Cajal-Retzius, or RADI cells of the lacunosum-molecular layer (Fuentealba et al., 2010), or the oriens-lacunosum-moleculare interneuron of the oriens layer (Klausberger et al., 2003).

The present study provides novel insights into the relationships between neurotransmitter receptor densities and expression levels of corresponding genes by analyzing tissue acquired from the same brain samples. Thus, we have overcome the limitation of previous studies which analyzed gene (Hawrylycz et al., 2012) and receptor (Zilles and Palomero-Gallagher, 2017) data obtained from different donors (Hansen et al., 2022a; Murgaš et al., 2022; Zachlod et al., 2022). However, there are a few other limitations to note. The first one is the rather small sample size due to the constraints resulting from the scarcity of human brain samples adequately fulfilling the technical requirements for autoradiography (e.g., unfixed fresh brain tissue (Palomero-Gallagher and Zilles, 2018)) and RNA quantification (e.g., postmortem interval (Lipska et al., 2006)). Of note, all tissue samples were processed in one batch to minimize potential bias through technical factors. The results of the effect size, statistical power, and cross validation confirmed the robustness and reliability of our findings. Given the relatively small sample size, follow-up analyses using additional non-overlapping samples would be required to further support our findings. Another technically-related limitation arises from the fact that the available radioligands cannot specifically label the subunits of ionotropic receptors or, in some cases, distinguish different subtypes of partial metabotropic receptors (Murgaš et al., 2022). For example, [^{3}H]-LY 341,495 labels both the mGluR2 and the mGluR3 receptors (Johnson et al., 1999), or [^{3}H]-prazosin does not distinguish between α_1 subtypes (Zilles et al., 1991). These issues motivate the development of novel ligands for the visualization of specific receptor subtypes, as well as of advanced methods to specifically identify the subunits of ionotropic receptors. A further limitation in the chosen approach for gene expression analysis is

that 3′mRNA-Seq reads mostly map to the last exon of genes and are thus not suited to determine transcript isoform expression (Ma et al., 2019), which might be differentially regulated between hippocampal regions (Park and Farris, 2021). Moreover, the present analysis has targeted the CA-region as a whole, although it can be further subdivided into areas CA1, CA2 and CA3, which differ in their receptor architecture, e.g. regarding the densities of AMPA, $GABA_A$ and $GABA_B$ receptors (Palomero-Gallagher et al., 2020). These regionally specific differences in densities may have an influence on the rather weak correlation found here. Such a combination into one region was necessary, however, since it is not possible to accurately identify and dissect the CA1, CA2 and CA3 regions on cryosections inside the cryotome. Finally, spatial transcriptomics would conserve the spatial information of cells within a tissue and would display gene expression profiles of individual cells, which provide a powerful method for the further study.

Concluding, using data obtained from the same brain samples, we could demonstrate that the regional-specific densities of neurotransmitter receptors and expression levels of their corresponding genes show a poor covariation in the human hippocampal CA and DG regions. Correlation coefficients between receptors and their corresponding genes vary widely depending on the different combinations between the receptor-gene types and the hippocampal regions. These data suggest that receptor expression is not only controlled by the corresponding RNA levels, but also mediated and modified by regionally specific functional differentiation, as well as by other multiple post-translational factors. Finally, the neurotransmitter receptor and corresponding gene data from the same brain samples constitute a valuable open resource for future studies and are made available via the EBRAINS platform (https://doi.org/10.25493/6BT0-BB1).

Data availability

All data are available in the main text, the supplementary materials, or the EBRAINS platform. Additional data related to this paper may be requested from the authors.

Declaration of Competing Interest

Authors declare that they have no competing interests.

Credit authorship contribution statement

Ling Zhao: Software, Formal analysis, Investigation, Data curation, Writing – original draft, Writing – review & editing, Visualization. **Thomas W. Mühleisen:** Formal analysis, Writing – original draft, Writing – review & editing, Visualization. **Dominique I. Pelzer:** Investigation, Writing – original draft, Writing – review & editing, Visualization. **Bettina Burger:** Investigation, Writing – review & editing. **Eva C. Beins:** Investigation. **Andreas J. Forstner:** Investigation, Writing – review & editing. **Stefan Herms:** Investigation. **Per Hoffmann:** Investigation. **Katrin Amunts:** Conceptualization, Resources, Writing – review & editing, Funding acquisition. **Nicola Palomero-Gallagher:** Conceptualization, Resources, Data curation, Writing – review & editing, Project administration, Funding acquisition. **Sven Cichon:** Conceptualization, Resources, Writing – review & editing, Project administration, Funding acquisition.

Acknowledgments

This article is dedicated to Professor Dr. med. Dr. h.c. Karl Zilles, deceased the 26th of April 2020. He was fully involved in the planning of the project, and we are greatly indebted to his neuroscientific legacy.

Funding

This project has received funding from the European Union's Horizon 2020 Research and Innovation Programme under the Specific Grant Agreement 945539 (Human Brain Project SGA3), and from the Helmholtz Association's Initiative and Networking Fund through the Helmholtz International BigBrain Analytics and Learning Laboratory (HIBALL) under the Helmholtz International Lab grant agreement InterLabs-0015 and from the Deutsche Forschungsgemeinschaft (DFG, German Research Foundation) under grant agreement 491111487.

Supplementary materials

Supplementary material associated with this article can be found, in the online version, at doi:10.1016/j.neuroimage.2023.120095.

References

Acsády, L., Káli, S., Scharfman, H.E., 2007. Models, structure, function: the transformation of cortical signals in the dentate gyrus. In: Progress in Brain Research. Elsevier, pp. 577–599.
Aggleton, J.P., Pralus, A., Nelson, A.J.D., Hornberger, M., 2016. Thalamic pathology and memory loss in early Alzheimer's disease: moving the focus from the medial temporal lobe to Papez circuit. Brain 139, 1877–1890.
Amunts, K., Mohlberg, H., Bludau, S., Zilles, K., 2020. Julich-brain: a 3D probabilistic atlas of the human brain's cytoarchitecture. Science 369, 988–992.
Amunts, K., Zilles, K., 2015. Architectonic mapping of the human brain beyond brodmann. Neuron 88, 1086–1107.
Battle, A., Khan, Z., Wang, S.H., Mitrano, A., Ford, M.J., Pritchard, J.K., Gilad, Y., 2015. Impact of regulatory variation from RNA to protein. Science 347, 664–667.
Berger, T., Lee, H., Young, A.H., Aarsland, D., Thuret, S., 2020. Adult hippocampal neurogenesis in major depressive disorder and alzheimer's disease. Trends Mol. Med. 26, 803–818.
Bernasconi, N., Bernasconi, A., Caramanos, Z., Antel, S.B., Andermann, F., Arnold, D.L., 2003. Mesial temporal damage in temporal lobe epilepsy: a volumetric MRI study of the hippocampus, amygdala and parahippocampal region. Brain 126, 462–469.
Bernhardt, B.C., Bernasconi, A., Liu, M., Hong, S.J., Caldairou, B., Goubran, M., Guiot, M.C., Hall, J., Bernasconi, N., 2016. The spectrum of structural and functional imaging abnormalities in temporal lobe epilepsy. Ann. Neuro. 80, 142–153.
Bernhardt, B.C., Hong, S.J., Bernasconi, A., Bernasconi, N., 2015. Magnetic resonance imaging pattern learning in temporal lobe epilepsy: classification and prognostics. Ann Neurol. 77, 436–446.
Biegon, A., Rainbow, T.C., Mann, J.J., McEwen, B.S., 1982. Neurotransmitter receptor sites in human hippocampus: a quantitative autoradiographic study. Brain Res. 247, 379–382.
Bludau, S., Mühleisen, T.W., Eickhoff, S.B., Hawrylycz, M.J., Cichon, S., Amunts, K., 2018. Integration of transcriptomic and cytoarchitectonic data implicates a role for MAOA and TAC1 in the limbic-cortical network. Brain Struct. Funct. 223, 2335–2342.
Blümcke, I., Thom, M., Aronica, E., Armstrong, D.D., Bartolomei, F., Bernasconi, A., Bernasconi, N., Bien, C.G., Cendes, F., Coras, R., Cross, J.H., Jacques, T.S., Kahane, P., Mathern, G.W., Miyata, H., Moshé, S.L., Oz, B., Özkara, Ç., Perucca, E., Sisodiya, S., Wiebe, S., Spreafico, R., 2013. International consensus classification of hippocampal sclerosis in temporal lobe epilepsy: a Task Force report from the ILAE commission on diagnostic methods. Epilepsia 54, 1315–1329.
Buccitelli, C., Selbach, M., 2020. mRNAs, proteins and the emerging principles of gene expression control. Nat. Rev. Genet. 21, 630–644.
Burt, J.B., Demirtaş, M., Eckner, W.J., Navejar, N.M., Ji, J.L., Martin, W.J., Bernacchia, A., Anticevic, A., Murray, J.D., 2018. Hierarchy of transcriptomic specialization across human cortex captured by structural neuroimaging topography. Nat. Neurosci. 21, 1251–1259.
Charan, J., Kantharia, N.D., 2013. How to calculate sample size in animal studies? J. Pharmacol. Pharmacother. 4, 303–306.
Cohen, J., 1992. A power primer. Psychol. Bull. 112, 155.
Collingridge, G.L., Isaac, J.T., Wang, Y.T., 2004. Receptor trafficking and synaptic plasticity. Nat. Rev. Neurosci. 5, 952–962.
Cox, M.A.A., Cox, T.F., Chen, C.H., Härdle, W., Unwin, A., 2008. Multidimensional scaling. In: Handbook of Data Visualization. Springer Berlin Heidelberg, Berlin, Heidelberg, pp. 315–347.
de Sousa Abreu, R., Penalva, L.O., Marcotte, E.M., Vogel, C., 2009. Global signatures of protein and mRNA expression levels. Mol. Biosyst. 5, 1512–1526.
Debski, K.J., Ceglia, N., Ghestem, A., Ivanov, A.I., Brancati, G.E., Broer, S., Bot, A.M., Muller, J.A., Schoch, S., Becker, A., Loscher, W., Guye, M., Sassone-Corsi, P., Lukasiuk, K., Baldi, P., Bernard, C., 2020. The circadian dynamics of the hippocampal transcriptome and proteome is altered in experimental temporal lobe epilepsy. Sci. Adv. 6, eaat5979.
Dieni, C.V., Panichi, R., Aimone, J.B., Kuo, C.T., Wadiche, J.I., Overstreet-Wadiche, L., 2016. Low excitatory innervation balances high intrinsic excitability of immature dentate neurons. Nat. Commun. 7, 11313.
Ferreira, J.S., Papouin, T., Ladépêche, L., Yao, A., Langlais, V.C., Bouchet, D., Dulong, J., Mothet, J.-P., Sacchi, S., Pollegioni, L., Paoletti, P., Oliet, S.H.R., Groc, L., 2017. Co-agonists differentially tune GluN2B-NMDA receptor trafficking at hippocampal synapses. Elife 6, e25492.
Fortelny, N., Overall, C.M., Pavlidis, P., Freue, G.V.C., 2017. Can we predict protein from mRNA levels? Nature 547, E19–E20.

Fuentealba, P., Klausberger, T., Karayannis, T., Suen, W.Y., Huck, J., Tomioka, R., Rockland, K., Capogna, M., Studer, M., Morales, M., Somogyi, P., 2010. Expression of COUP-TFII nuclear receptor in restricted GABAergic neuronal populations in the adult rat hippocampus. J. Neurosci. 30, 1595–1609.

Graebenitz, S., Kedo, O., Speckmann, E.J., Gorji, A., Panneck, H., Hans, V., Palomero–Gallagher, N., Schleicher, A., Zilles, K., Pape, H.C., 2011. Interictal-like network activity and receptor expression in the epileptic human lateral amygdala. Brain 134, 2929–2947.

Greger, I.H., Watson, J.F., Cull-Candy, S.G., 2017. Structural and functional architecture of AMPA-type glutamate receptors and their auxiliary proteins. Neuron 94, 713–730.

Groc, L., Choquet, D., 2020. Linking glutamate receptor movements and synapse function. Science 368, eaay4631.

Gry, M., Rimini, R., Strömberg, S., Asplund, A., Pontén, F., Uhlén, M., Nilsson, P., 2009. Correlations between RNA and protein expression profiles in 23 human cell lines. BMC Genom. 10, 1–14.

Gulyás, A.I., Tóth, K., McBain, C.J., Freund, T.F., 1998. Stratum radiatum giant cells: a type of principal cell in the rat hippocampus. Eur. J. Neurosci. 10, 3813–3822.

Hall, J.E., Hall, M.E., 2020. Guyton and Hall textbook of Medical Physiology, 14th ed. Elsevier Health Sciences, Philadelphia, PA.

Hansen, J.Y., Markello, R.D., Tuominen, L., Nørgaard, M., Kuzmin, E., Palomero-Gallagher, N., Dagher, A., Misic, B., 2022a. Correspondence between gene expression and neurotransmitter receptor and transporter density in the human brain. Neuroimage 264, 119671.

Hansen, J.Y., Shafiei, G., Markello, R.D., Smart, K., Cox, S.M.L., Nørgaard, M., Beliveau, V., Wu, Y., Gallezot, J.-.D., Aumont, É., Servaes, S., Scala, S.G., DuBois, J.M., Wainstein, G., Bezgin, G., Funck, T., Schmitz, T.W., Spreng, R.N., Galovic, M., Koepp, M.J., Duncan, J.S., Coles, J.P., Fryer, T.D., Aigbirhio, F.I., McGinnity, C.J., Hammers, A., Soucy, J.P., Baillet, S., Guimond, S., Hietala, J., Bedard, M.A., Leyton, M., Kobayashi, E., Rosa-Neto, P., Ganz, M., Knudsen, G.M., Palomero-Gallagher, N., Shine, J.M., Carson, R.E., Tuominen, L., Dagher, A., Misic, B., 2022b. Mapping neurotransmitter systems to the structural and functional organization of the human neocortex. Nat Neurosci.

Haselmann, H., Mannara, F., Werner, C., Planagumà, J., Miguez-Cabello, F., Schmidl, L., Grünewald, B., Petit-Pedrol, M., Kirmse, K., Classen, J., Demir, F., Klöcker, N., Soto, D., Doose, S., Dalmau, J., Hallermann, S., Geis, C., 2018. Human Autoantibodies against the AMPA receptor subunit GluA2 induce receptor reorganization and memory dysfunction. Neuron 100, 91–105 e109.

Hawrylycz, M., Miller, J.A., Menon, V., Feng, D., Dolbeare, T., Guillozet-Bongaarts, A.L., Jegga, A.G., Aronow, B.J., Lee, C.K., Bernard, A., Glasser, M.F., Dierker, D.L., Menche, J., Szafer, A., Collman, F., Grange, P., Berman, K.A., Mihalas, S., Yao, Z., Stewart, L., Barabási, A.L., Schulkin, J., Phillips, J., Ng, L., Dang, C., Haynor, D.R., Jones, A., Van Essen, D.C., Koch, C., Lein, E., 2015. Canonical genetic signatures of the adult human brain. Nat. Neurosci. 18, 1832–1844.

Hawrylycz, M.J., Lein, E.S., Guillozet-Bongaarts, A.L., Shen, E.H., Ng, L., Miller, J.A., van de Lagemaat, L.N., Smith, K.A., Ebbert, A., Riley, Z.L., Abajian, C., Beckmann, C.F., Bernard, A., Bertagnolli, D., Boe, A.F., Cartagena, P.M., Chakravarty, M.M., Chapin, M., Chong, J., Dalley, R.A., Daly, B.D., Dang, C., Datta, S., Dee, N., Dolbeare, T.A., Faber, V., Feng, D., Fowler, D.R., Goldy, J., Gregor, B.W., Haradon, Z., Haynor, D.R., Hohmann, J.G., Horvath, S., Howard, R.E., Jeromin, A., Jochim, J.M., Kinnunen, M., Lau, C., Lazarz, E.T., Lee, C., Lemon, T.A., Li, L., Li, Y., Morris, J.A., Overly, C.C., Parker, P.D., Parry, S.E., Reding, M., Royall, J.J., Schulkin, J., Sequeira, P.A., Slaughterbeck, C.R., Smith, S.C., Sodt, A.J., Sunkin, S.M., Swanson, B.E., Vawter, M.P., Williams, D., Wohnoutka, P., Zielke, H.R., Geschwind, D.H., Hof, P.R., Smith, S.M., Koch, C., Grant, S.G.N., Jones, A.R., 2012. An anatomically comprehensive atlas of the adult human brain transcriptome. Nature 489, 391–399.

Hogan, R.E., Wang, L., Bertrand, M.E., Willmore, L.J., Bucholz, R.D., Nassif, A.S., Csernansky, J.G., 2004. MRI-based high-dimensional hippocampal mapping in mesial temporal lobe epilepsy. Brain 127, 1731–1740.

Hood, J.L., Emeson, R.B., 2011. Editing of neurotransmitter receptor and ion channel RNAs in the nervous system. Curr. Top. Microbiol. Immunol. 61–90.

Impieri, D., Zilles, K., Niu, M., Rapan, L., Schubert, N., Galletti, C., Palomero-Gallagher, N., 2019. Receptor density pattern confirms and enhances the anatomic-functional features of the macaque superior parietal lobule areas. Brain Struct. Funct. 224, 2733–2756.

Isaac, J.T.R., Ashby, M.C., McBain, C.J., 2007. The role of the gluR2 subunit in AMPA receptor function and synaptic plasticity. Neuron 54, 859–871.

Johnson, B.G., Wright, R.A., Arnold, M.B., Wheeler, W.J., Ornstein, P.L., Schoepp, D.D., 1999. [3H]-LY341495 as a novel antagonist radioligand for group II metabotropic glutamate (mGlu) receptors: characterization of binding to membranes of mGlu receptor subtype expressing cells. Neuropharmacology 38, 1519–1529.

Keren, H., Lev-Maor, G., Ast, G., 2010. Alternative splicing and evolution: diversification, exon definition and function. Nat Rev Genet 11, 345–355.

Khan, A.F., Adewale, Q., Baumeister, T.R., Carbonell, F., Zilles, K., Palomero-Gallagher, N., Iturria-Medina, Y., Alzheimer's Disease Neuroimaging, I., 2021. Personalized brain models identify neurotransmitter receptor changes in Alzheimer's disease. Brain awab375.

Klausberger, T., Magill, P.J., Márton, L.F., Roberts, J.D., Cobden, P.M., Buzsáki, G., Somogyi, P., 2003. Brain-state- and cell-type-specific firing of hippocampal interneurons *in vivo*. Nature 421, 844–848.

Kliouevа, N.M., Rademaker, M.C., Huitinga, I., Huitinga, I., Webster, M.J., 2018. Design of a European code of conduct for brain banking. In: Handbook of Clinical Neurology. Elsevier, pp. 51–81.

Levitz, J., Habrian, C., Bharill, S., Fu, Z., Vafabakhsh, R., Isacoff, E.Y., 2016. Mechanism of assembly and cooperativity of homomeric and heteromeric metabotropic glutamate receptors. Neuron 92, 143–159.

Lipska, B.K., Deep-Soboslay, A., Weickert, C.S., Hyde, T.M., Martin, C.E., Herman, M.M., Kleinman, J.E., 2006. Critical factors in gene expression in postmortem human brain: focus on studies in schizophrenia. Biol. Psychiatry 60, 650–658.

Liu, Y., Beyer, A., Aebersold, R., 2016. On the dependency of cellular protein levels on mRNA abundance. Cell 165, 535–550.

Ma, F., Fuqua, B.K., Hasin, Y., Yukhtman, C., Vulpe, C.D., Lusis, A.J., Pellegrini, M., 2019. A comparison between whole transcript and 3' RNA sequencing methods using Kapa and Lexogen library preparation methods. BMC Genom. 20, 9.

Malinow, R., Malenka, R.C., 2002. AMPA receptor trafficking and synaptic plasticity. Annu. Rev. Neurosci. 25, 103–126.

Merker, B., 1983. Silver staining of cell bodies by means of physical development. J. Neurosci. Methods 9, 235–241.

Murgaš, M., Michenthaler, P., Reed, M.B., Gryglewski, G., Lanzenberger, R., 2022. Correlation of receptor density and mRNA expression patterns in the human cerebral cortex. Neuroimage 256, 119214.

Nichols, T.E., Holmes, A.P., 2002. Nonparametric permutation tests for functional neuroimaging: a primer with examples. Hum. Brain Mapp. 15, 1–25.

Palomero-Gallagher, N., Kedo, O., Mohlberg, H., Zilles, K., Amunts, K., 2020. Multimodal mapping and analysis of the cyto- and receptorarchitecture of the human hippocampus. Brain Struct. Funct. 225, 881–907.

Palomero-Gallagher, N., Schleicher, A., Bidmon, H.J., Pannek, H.W., Hans, V., Gorji, A., Speckmann, E.-.J., Zilles, K., 2012. Multireceptor analysis in human neocortex reveals complex alterations of receptor ligand binding in focal epilepsies. Epilepsia 53, 1987–1997.

Palomero-Gallagher, N., Zilles, K., Huitinga, I., Webster, M.J., 2018. Cyto- and receptor architectonic mapping of the human brain. In: Handbook of Clinical Neurology. Elsevier, pp. 355–387.

Paoletti, P., Neyton, J., 2007. NMDA receptor subunits: function and pharmacology. Curr. Opin. Pharmacol. 7, 39–47.

Papez, J.W., 1937. A proposed mechanism of emotion. Arch. Neurol. Psychiatry 38, 725–743.

Park, J., Farris, S., 2021. Spatiotemporal regulation of transcript isoform expression in the hippocampus. Front. Mol. Neurosci. 14, 694234.

Payne, S.H., 2015. The utility of protein and mRNA correlation. Trends Biochem. Sci. 40, 1–3.

Perry, E.K., Court, J.A., Johnson, M., Smith, C.J., James, V., Cheng, A.V., Kerwin, J.M., Morris, C.M., Piggott, M.A., Edwardson, J.A., Birdsall, N.J.M., Turner, J.T., Perry, R.H., 1993. Autoradiographic comparison of cholinergic and other transmitter receptors in the normal human hippocampus. Hippocampus 3, 307–315.

Robinson, M.D., Oshlack, A., 2010. A scaling normalization method for differential expression analysis of RNA-seq data. Genome Biol. 11, R25.

Schober, P., Boer, C., Schwarte, L.A., 2018. Correlation coefficients: appropriate use and interpretation. Anesth. Analg. 126, 1763–1768.

Scholtens, L.H., Schmidt, R., de Reus, M.A., van den Heuvel, M.P., 2014. Linking macroscale graph analytical organization to microscale neuroarchitectonics in the macaque connectome. J. Neurosci. 34, 12192.

Schulz, H., Ruppert, A.-.K., Herms, S., Wolf, C., Mirza-Schreiber, N., Stegle, O., Czamara, D., Forstner, A.J., Sivalingam, S., Schoch, S., Moebus, S., Pütz, B., Hillmer, A., Fricker, N., Vatter, H., Müller-Myhsok, B., Nöthen, M.M., Becker, A.J., Hoffmann, P., Sander, T., Cichon, S., 2017. Genome-wide mapping of genetic determinants influencing DNA methylation and gene expression in human hippocampus. Nat. Commun. 8, 1511.

Schurger, A., Pereira, F., Treisman, A., Cohen Jonathan, D., 2010. Reproducibility distinguishes conscious from nonconscious neural representations. Science 327, 97–99.

Schwanhäusser, B., Busse, D., Li, N., Dittmar, G., Schuchhardt, J., Wolf, J., Chen, W., Selbach, M., 2011. Global quantification of mammalian gene expression control. Nature 473, 337–342.

Schwappach, B., 2008. An overview of trafficking and assembly of neurotransmitter receptors and ion channels (Review). Mol. Membr. Biol. 25, 270–278.

Selkoe, D.J., 2001. Alzheimer's disease: genes, proteins, and therapy. Physiol. Rev. 81, 741–766.

Somogyi, J., Szabo, A., Somogyi, P., Lamsa, K., 2012. Molecular analysis of ivy cells of the hippocampal CA1 stratum radiatum using spectral identification of immunofluorophores. Front. Neural Circuits 6.

Stephenson, F.A., Cousins, S.L., Kenny, A.V., 2008. Assembly and forward trafficking of NMDA receptors (Review). Mol. Membr. Biol. 25, 311–320.

Symonds, J.D., Zuberi, S.M., Johnson, M.R., 2017. Advances in epilepsy gene discovery and implications for epilepsy diagnosis and treatment. Curr. Opin. Neurol. 30.

Szot, P., White, S.S., Greenup, J.L., Leverenz, J.B., Peskind, E.R., Raskind, M.A., 2005. α1-Adrenoreceptor in human hippocampus: binding and receptor subtype mRNA expression. Brain Res. Mol. Brain Res. 139, 367–371.

Thom, M., 2014. Review: hippocampal sclerosis in epilepsy: a neuropathology review. Neuropathol. Appl. Neurobiol. 40, 520–543.

Tremblay, E., Represa, A., Ben-Ari, Y., 1985. Autoradiographic localization of kainic acid binding sites in the human hippocampus. Brain Res. 343, 378–382.

van Strien, N.M., Cappaert, N.L.M., Witter, M.P., 2009. The anatomy of memory: an interactive overview of the parahippocampal–hippocampal network. Nat. Rev. Neurosci. 10, 272–282.

Vogel, C., de Sousa Abreu, R., Ko, D., Le, S.Y., Shapiro, B.A., Burns, S.C., Sandhu, D., Boutz, D.R., Marcotte, E.M., Penalva, L.O., 2010. Sequence signatures and mRNA concentration can explain two-thirds of protein abundance variation in a human cell line. Mol. Syst. Biol. 6, 400.

Vogel, C., Marcotte, E.M., 2012. Insights into the regulation of protein abundance from proteomic and transcriptomic analyses. Nat. Rev. Genet. 13, 227–232.

Vogel, J.W., La Joie, R., Grothe, M.J., Diaz-Papkovich, A., Doyle, A., Vachon-Presseau, E., Lepage, C., Vos de Wael, R., Thomas, R.A., Iturria-Medina, Y., Bernhardt, B., Rabinovici, G.D., Evans, A.C., 2020. A molecular gradient along the longitudinal axis of the human hippocampus informs large-scale behavioral systems. Nat. Commun. 11, 960.

Wang, D., Eraslan, B., Wieland, T., Hallström, B., Hopf, T., Zolg, D.P., Zecha, J., Asplund, A., Li, L.H., Meng, C., Frejno, M., Schmidt, T., Schnatbaum, K., Wilhelm, M., Ponten, F., Uhlen, M., Gagneur, J., Hahne, H., Kuster, B., 2019. A deep proteome and transcriptome abundance atlas of 29 healthy human tissues. Mol. Syst. Biol. 15, e8503.

Yadav, R., Dravid, S.M., Yuan, H., Traynelis, S.F., 2017. AMPA Receptors: Molecular Biology and Pharmacology☆. The Curated Reference Collection in Neuroscience and Biobehavioral Psychology. Elsevier Science Ltd.

Yao, Z., van Velthoven, C.T.J., Nguyen, T.N., Goldy, J., Sedeno-Cortes, A.E., Baftizadeh, F., Bertagnolli, D., Casper, T., Chiang, M., Crichton, K., Ding, S.L., Fong, O., Garren, E., Glandon, A., Gouwens, N.W., Gray, J., Graybuck, L.T., Hawrylycz, M.J., Hirschstein, D., Kroll, M., Lathia, K., Lee, C., Levi, B., McMillen, D., Mok, S., Pham, T., Ren, Q., Rimorin, C., Shapovalova, N., Sulc, J., Sunkin, S.M., Tieu, M., Torkelson, A., Tung, H., Ward, K., Dee, N., Smith, K.A., Tasic, B., Zeng, H., 2021. A taxonomy of transcriptomic cell types across the isocortex and hippocampal formation. Cell 184, 3222–3241 e3226.

Zachlod, D., Bludau, S., Cichon, S., Palomero-Gallagher, N., Amunts, K., 2022. Combined analysis of cytoarchitectonic, molecular and transcriptomic patterns reveal differences in brain organization across human functional brain systems. Neuroimage 257, 119286.

Zhang, B., Wang, J., Wang, X., Zhu, J., Liu, Q., Shi, Z., Chambers, M.C., Zimmerman, L.J., Shaddox, K.F., Kim, S., Davies, S.R., Wang, S., Wang, P., Kinsinger, C.R., Rivers, R.C., Rodriguez, H., Townsend, R.R., Ellis, M.J.C., Carr, S.A., Tabb, D.L., Coffey, R.J., Slebos, R.J.C., Liebler, D.C., Carr, S.A., Gillette, M.A., Klauser, K.R., Kuhn, E., Mani, D.R., Mertins, P., Ketchum, K.A., Paulovich, A.G., Whiteaker, J.R., Edwards, N.J., McGarvey, P.B., Madhavan, S., Wang, P., Chan, D., Pandey, A., Shih, I.-.M., Zhang, H., Zhang, Z., Zhu, H., Whiteley, G.A., Skates, S.J., White, F.M., Levine, D.A., Boja, E.S., Kinsinger, C.R., Hiltke, T., Mesri, M., Rivers, R.C., Rodriguez, H., Shaw, K.M., Stein, S.E., Fenyo, D., Liu, T., McDermott, J.E., Payne, S.H., Rodland, K.D., Smith, R.D., Rudnick, P., Snyder, M., Zhao, Y., Chen, X., Ransohoff, D.F., Hoofnagle, A.N., Liebler, D.C., Sanders, M.E., Shi, Z., Slebos, R.J.C., Tabb, D.L., Zhang, B., Zimmerman, L.J., Wang, Y., Davies, S.R., Ding, L., Ellis, M.J.C., Reid Townsend, R.the, N.C., National Cancer Institute Clinical Proteomics Tumor Analysis, C., 2014. Proteogenomic characterization of human colon and rectal cancer. Nature 513, 382–387.

Zhong, S., Ding, W., Sun, L., Lu, Y., Dong, H., Fan, X., Liu, Z., Chen, R., Zhang, S., Ma, Q., Tang, F., Wu, Q., Wang, X., 2020. Decoding the development of the human hippocampus. Nature 577, 531–536.

Zilles, K., Gross, G., Schleicher, A., Schildgen, S., Bauer, A., Bahro, M., Schwendemann, G., Zech, K., Kolassa, N., 1991. Regional and laminar distributions of α1-adrenoceptors and their subtypes in human and rat hippocampus. Neuroscience 40, 307–320.

Zilles, K., Palomero-Gallagher, N., 2017. Multiple transmitter receptors in regions and layers of the human cerebral cortex. Front. Neuroanat. 11, 78.

Zilles, K., Schleicher, A., Palomero-Gallagher, N., Amunts, K., Toga, A.W., Mazziotta, J.C., 2002. Quantitative analysis of cyto- and receptor architecture of the human brain. In: Brain Mapping: The Methods (Second Edition). Academic Press, San Diego, pp. 573–602.

Supplementary Material

Supplementary Material and Methods:

Comparison of gene expression using data from the Allen Human Brain Atlas

To follow-up results of receptor encoding genes, RNA expression differences between CA and DG were analyzed using JuGEx (Bludau et al., 2018), a freely accessible tool (https://www.fz-juelich.de/inm/inm-1/jugex) based on scripts coded in MATLAB (version R2018b, 64 bit; The MathWorks) which integrates regional RNA data from samples of the Allen Human Brain Atlas (Hawrylycz et al., 2015; Hawrylycz et al., 2012) with three-dimensional cytoarchitectonic probability maps from the Julich-Brain Atlas (Amunts et al., 2020), whereby the donor data do not overlap between both atlas systems.

Since tissue samples obtained via the Netherlands Brain Bank only encompassed an approximately 1 cm slab taken from the rostral third of the hippocampal body, we modified the cytoarchitectonic probability maps of the CA1-CA3 and DG regions (Palomero-Gallagher et al., 2020) to create volumes of interest (VOI) comparable in location and extent to that of the tissue from which we obtained our receptor density and gene expression data. For the CA-VOI, the probability maps of the CA1-CA3 regions from both hemispheres were merged, and the ensuing volume was cropped in the rostral and caudal directions to create a slab located in the rostral third of the hippocampal body. For the DG-VOI, the DG probabilistic map was also cropped in the rostral and caudal directions to match the rostro-caudal extent of the CA-VOI. We used a semantic filter within the JuGEx tool to eliminate the possibility that both maps used the same tissue block. For CA we used the Allen Human Brain Atlas terms: “CA1 field”, “CA2 field “and “CA3 field”. DG includes the Allen Human Brain Atlas labels: “CA4 field” and “dentate gyrus”. Our adjusted CA-VOI included 13 tissue samples from 5 brains of the Allen Human Brain Atlas, and the adjusted DG-VOI encompassed 5 tissue samples from three brains. The spatial assignment of

tissue samples to the CA- and DG-VOIs was manually checked using the "3D visualization" GUI of JuGEx (**Supplementary Fig. S7**).

The differential expression of a receptor-subunit encoding gene was defined as a significantly higher expression (z-score) in CA-VOI compared to DG-VOI. To address all transcript isoforms of a gene represented by the Allen Atlas, analyses were performed using JuGEx's "all-probes mode". We considered a *p*-value smaller than 0.05 as a significant difference between the z-scores of tissue samples in the CA- and DG-VOIs. The nominal *p*-values from the n-way analysis of variance (ANOVA) were corrected for multiple comparisons by a partial Bonferroni correction method (Scholtens et al., 2014).

Supplementary Fig. S1. Schematic representation of the experimental setup followed in the present study.

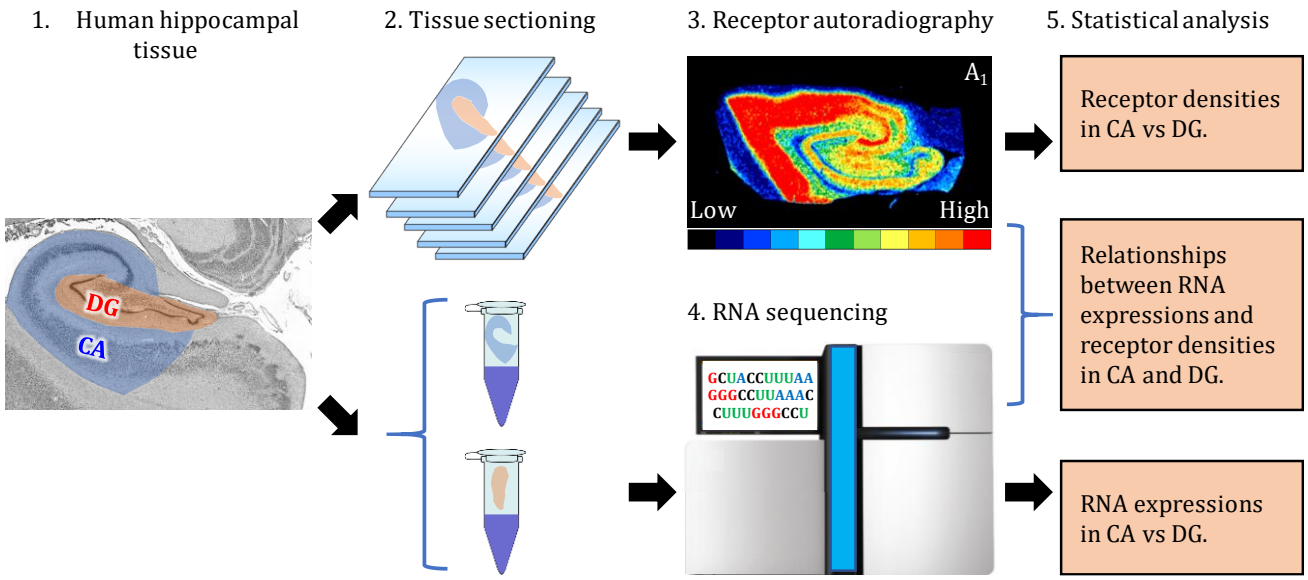

Supplementary Fig. S2. Overall sample similarity was analyzed using principal component analysis (PCA) of normalized gene counts (CPM, log2-transformed). One sample was identified as an outlier and was excluded from further analysis.

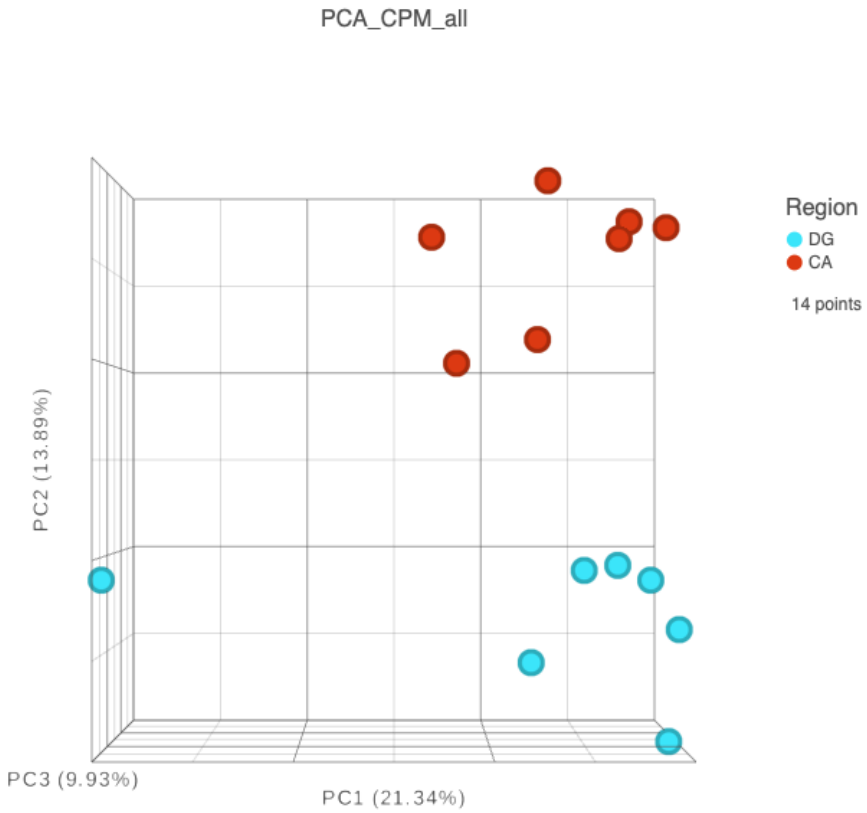

Supplementary Fig. S3. (A) Poor congruent receptor-gene alignment between DG and CA. X-axis is correlation between each receptor density and corresponding gene expression level in CA and Y-axis is that in DG. The receptor name in figure represents the correlation coefficient between receptor density and corresponding gene expression level. The correlation was computed by first averaging the main subunit gene expressions for a given receptor type for each subject (**Supplementary Table S7**) before running the within-gene correlation analysis. The ensuing correlation coefficients are provided in **Supplementary Table S8**. (B) Relationships between RNA expression levels and receptor densities across metabotropic receptor encoding genes in CA and DG, respectively. The mean densities of metabotropic receptors and expression levels of corresponding genes were provided in **Supplementary Tables S3 and S4.**

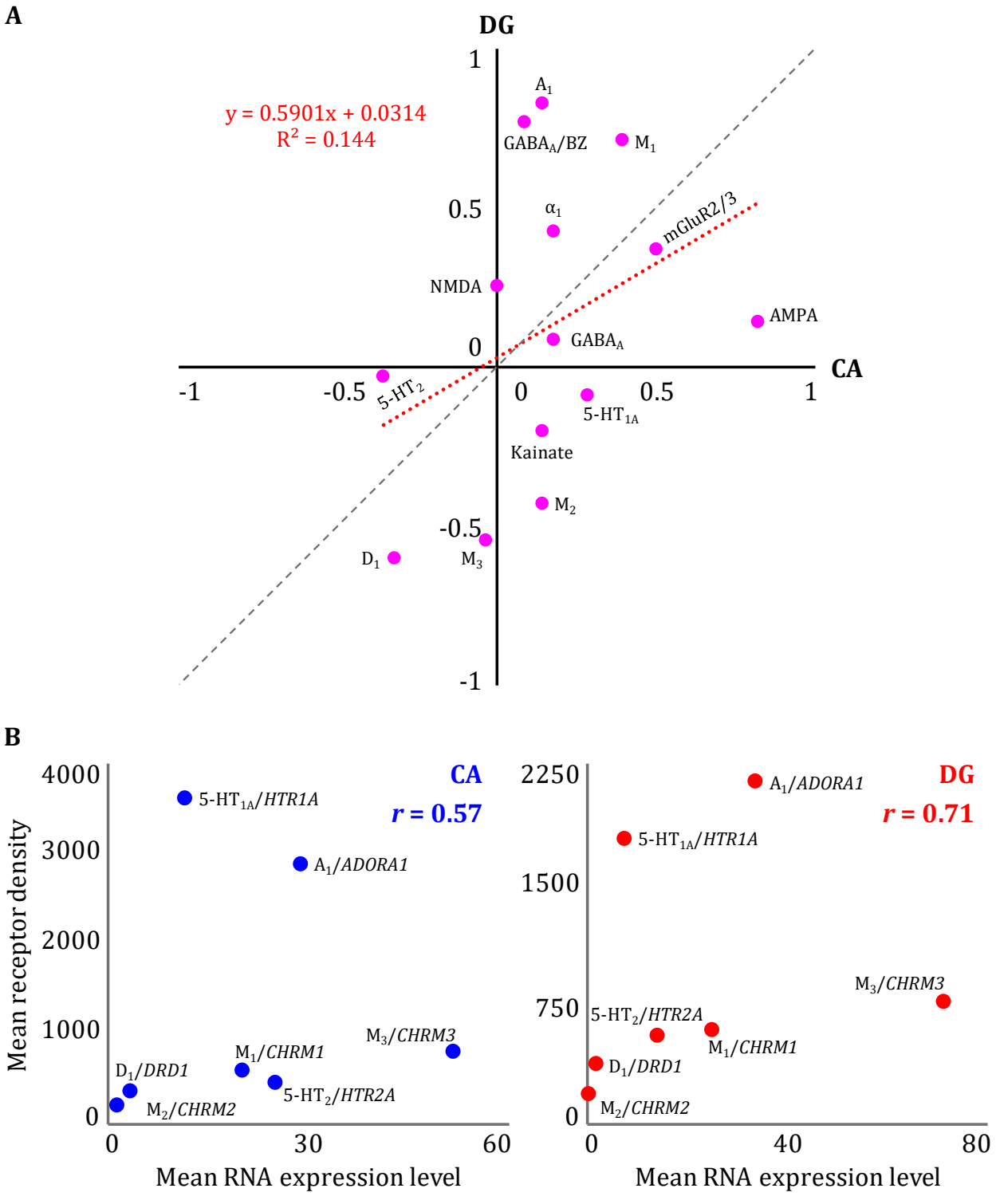

Supplementary Fig. S4. Venn diagram shows the overlapping genes between the 17 genes showing significantly different expression levels between CA and DG (G-CA/DG subset), the 15 genes presenting high-strength correlations with corresponding receptors in CA (G/R-CA subset), and the 24 genes with high-strength correlations in DG (G/R-DG subset). More detailed information of these genes is presented in **Supplementary Table S9**. Abbreviation: G, gene; R, receptor.

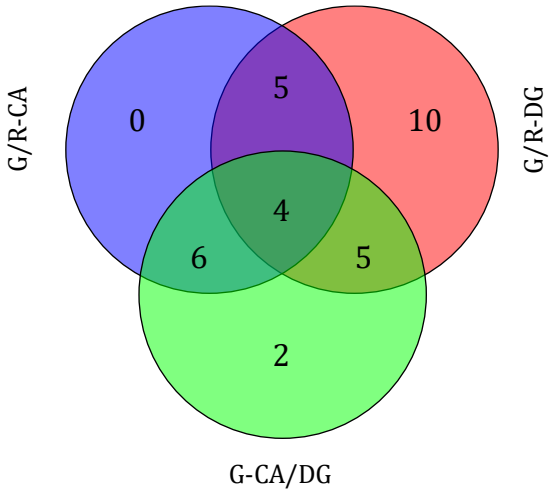

Supplementary Fig. S5. Relationships between the densities of each of the analyzed receptor types and the expression levels of their corresponding genes in the human *Cornu Ammonis* (CA) and dentate gyrus (DG).

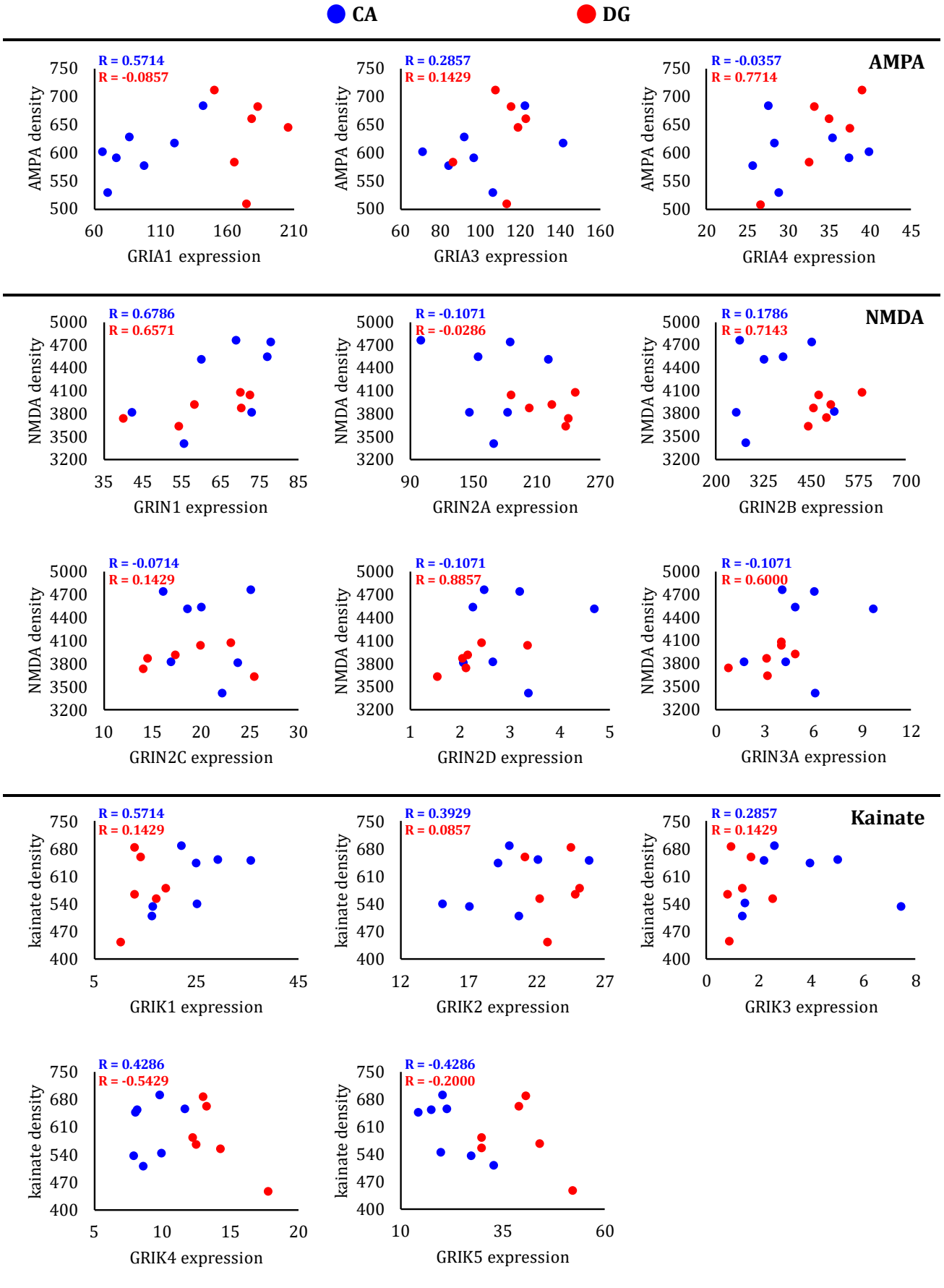

Supplementary Fig. S5 (continued).

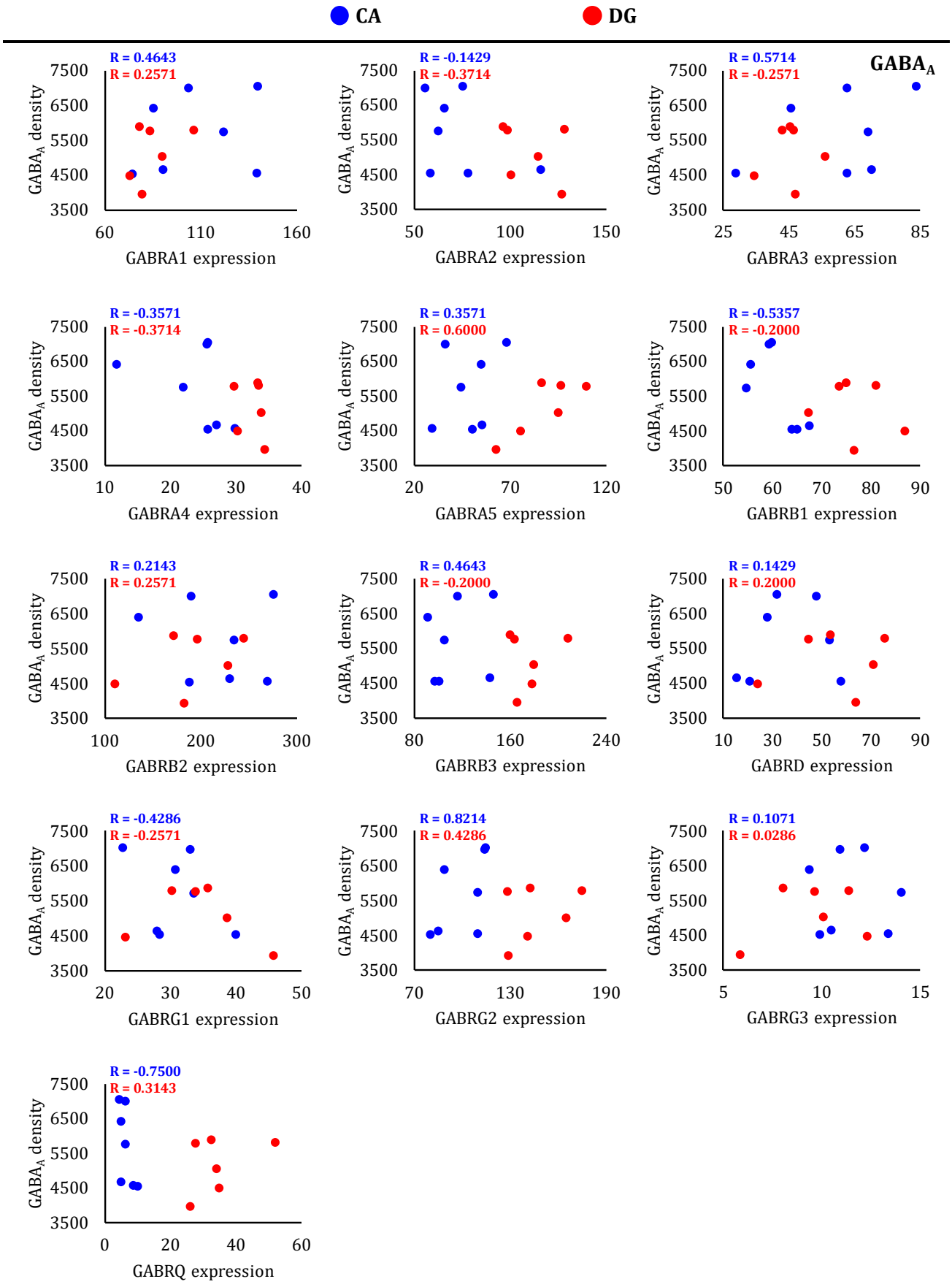

Supplementary Fig. S5 (continued).

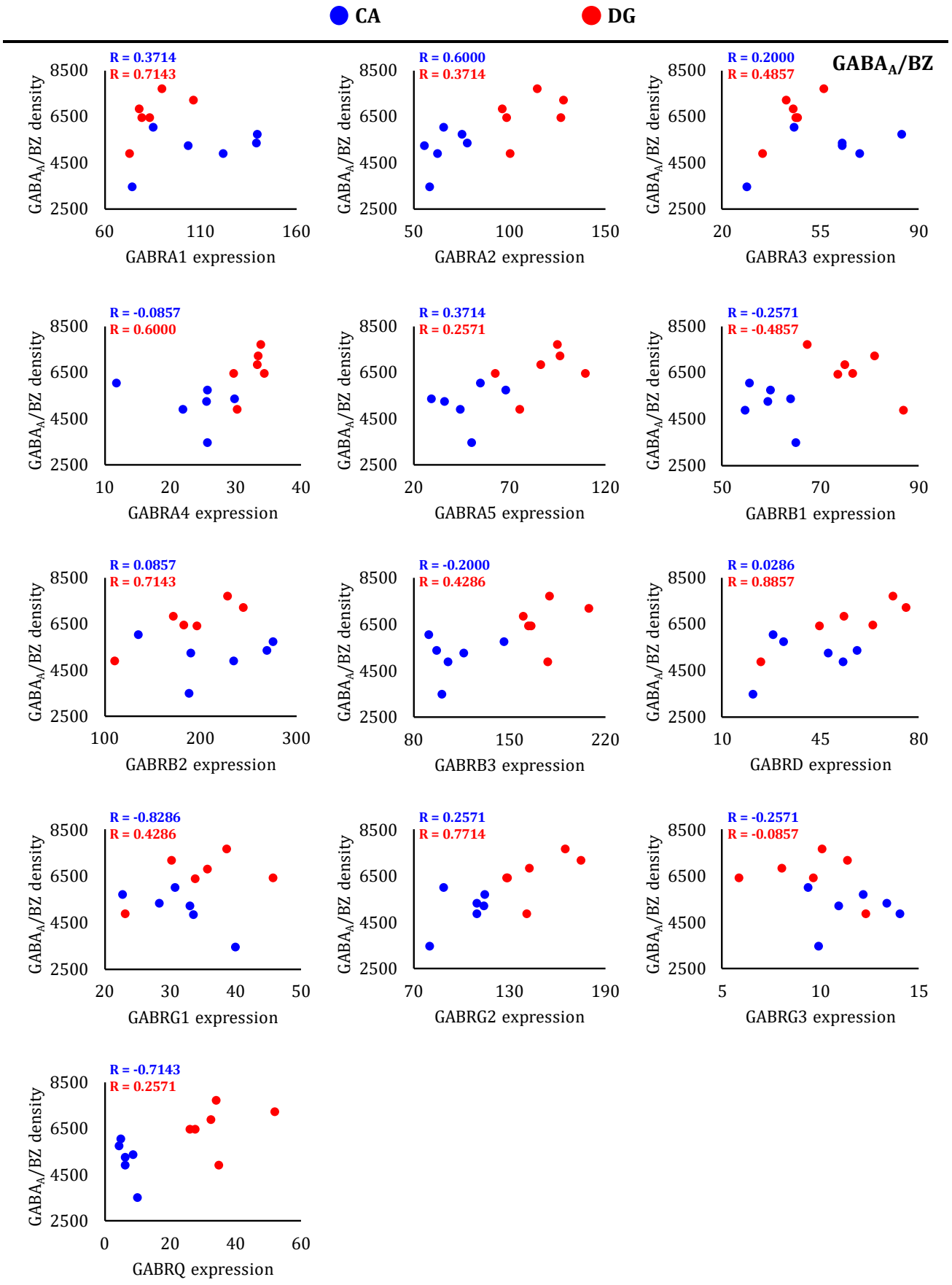

Supplementary Fig. S5 (continued).

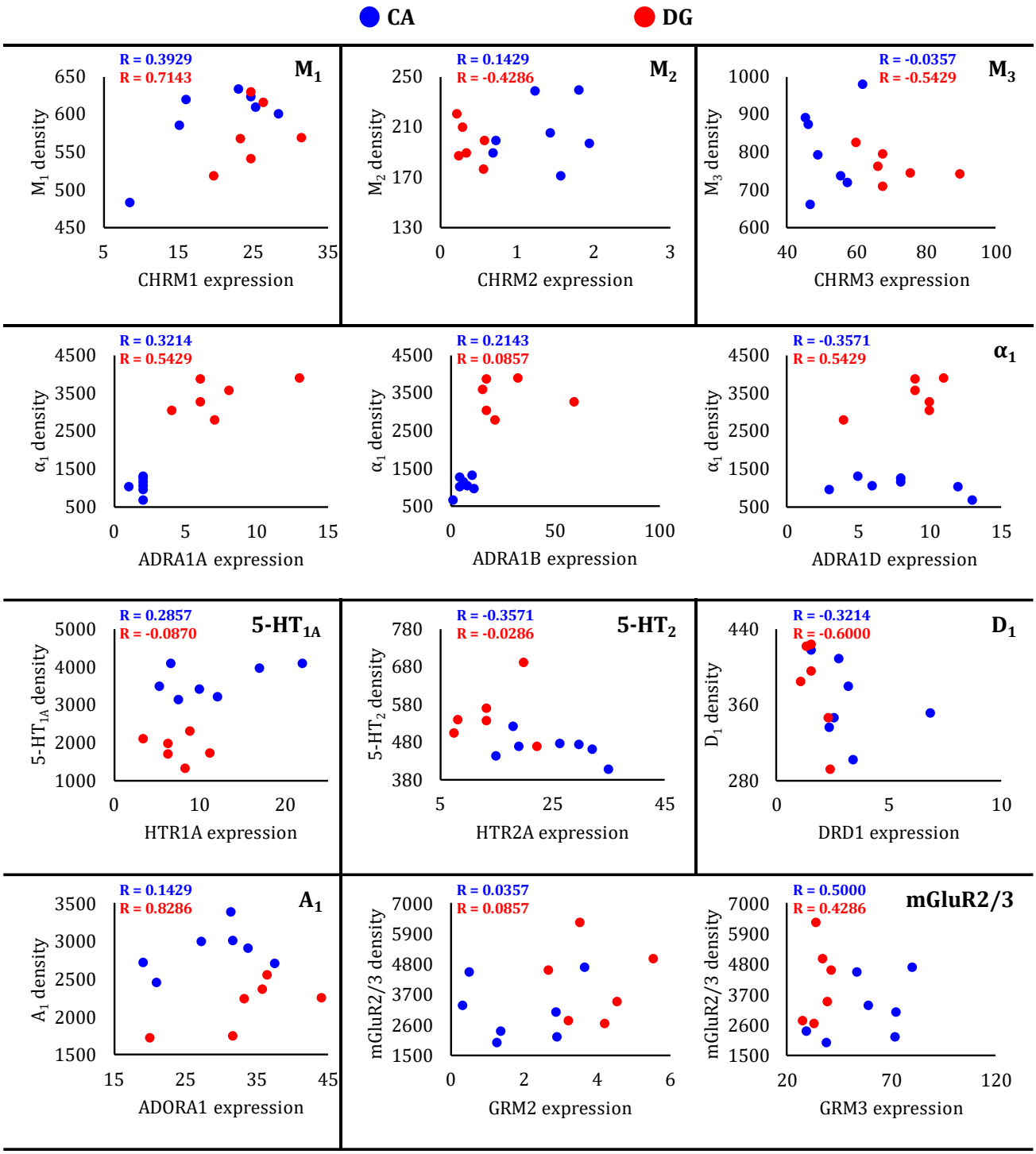

Supplementary Fig. S6. Multidimensional analyses (MDS) based on the Spearman rank correlation coefficients between the different analyzed receptor types (each represented by the black circle) and their corresponding genes.

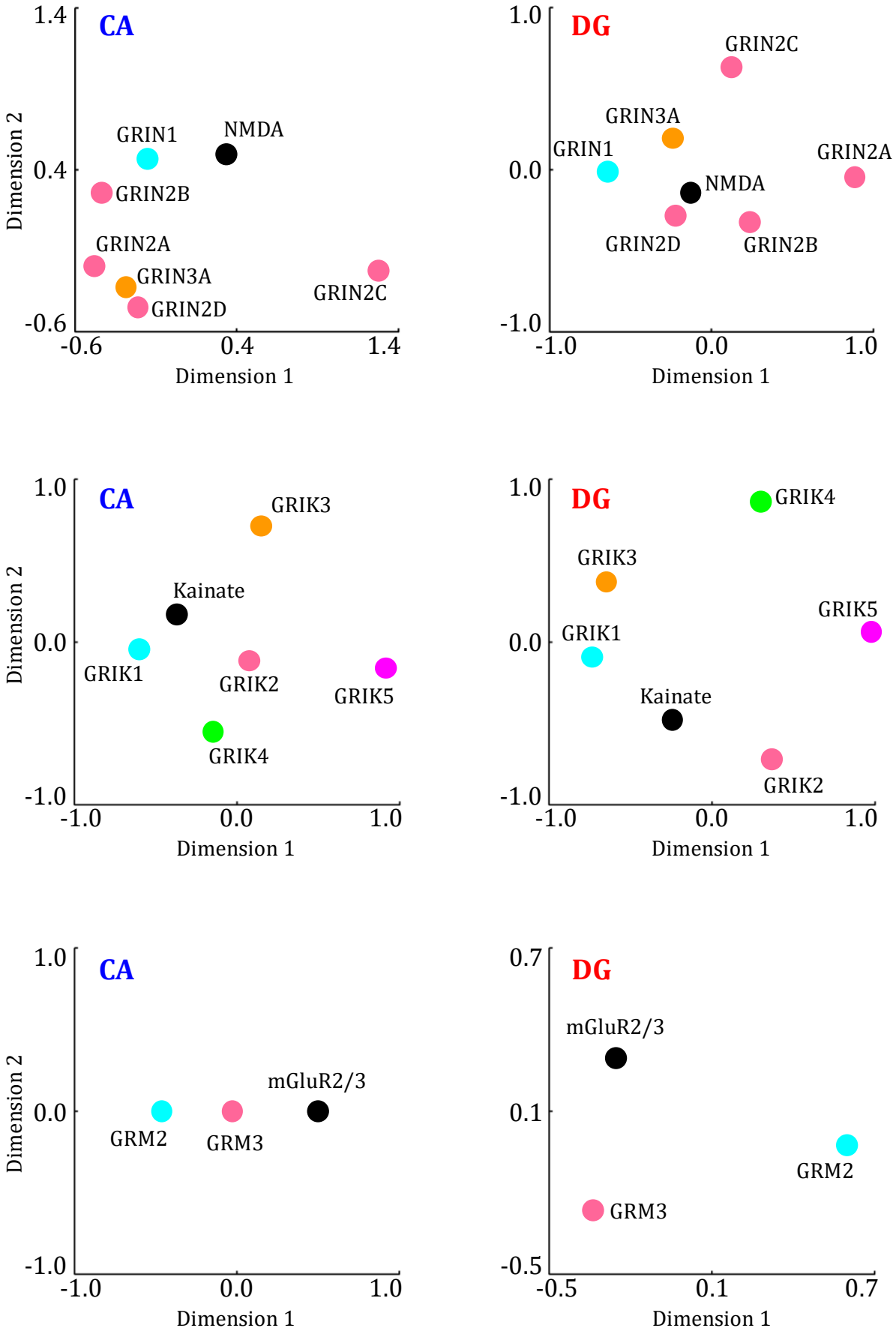

Supplementary Fig. S6 (continued).

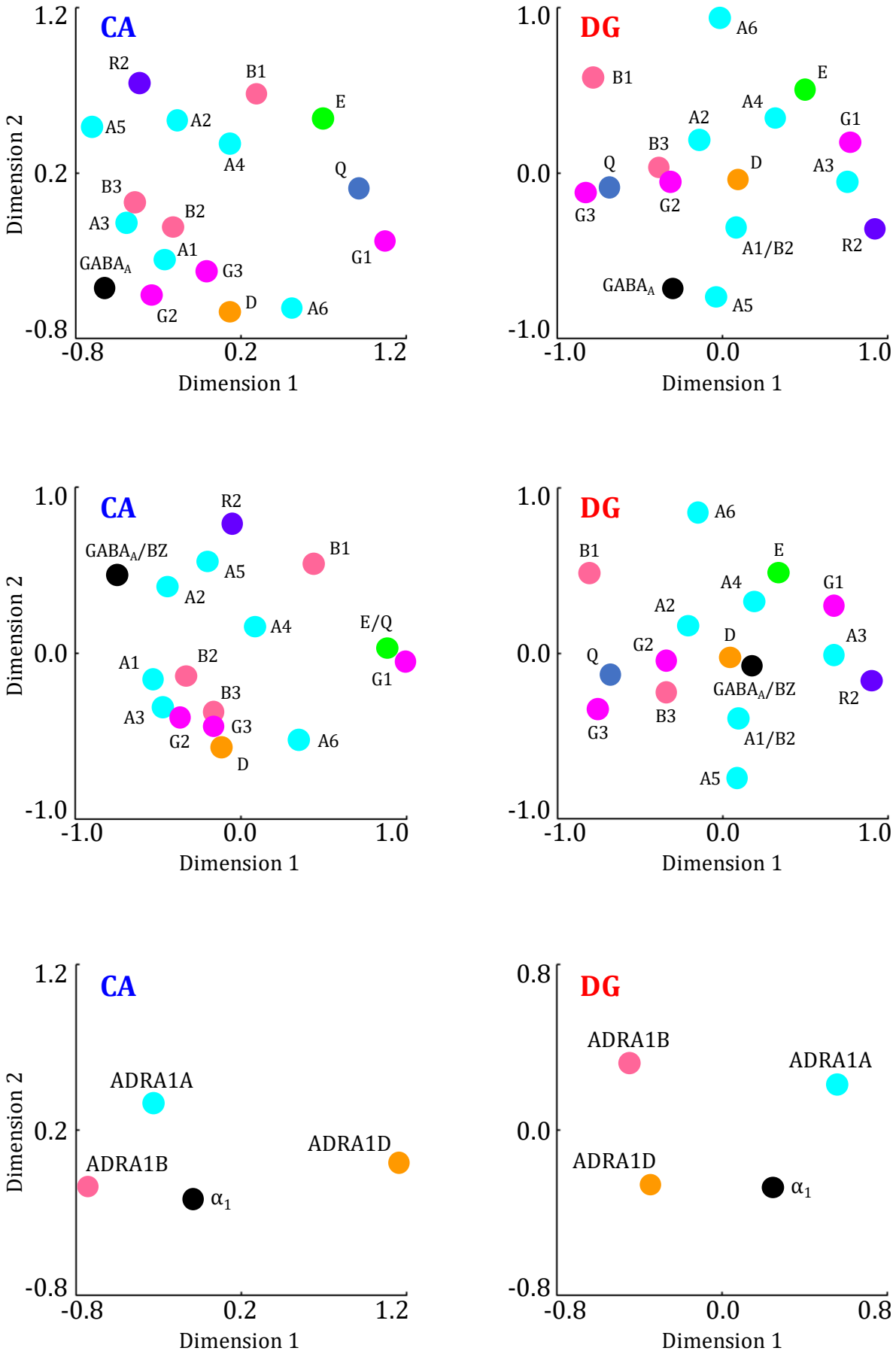

Supplementary Fig. S7. 3D visualization of the gene expression analysis using JuGEx in a ventral view (left panel) and a lateral view (right panel). For example, the expression level of gene *GRIA2* was analyzed between the adapted CA region (in red) and the adapted DG region (in blue). Investigated tissue samples are represented by spheres in CA and crosses in DG. RNA expression levels are indicated by z-scores showing ranges between maximal (green) and minimal values (pink).

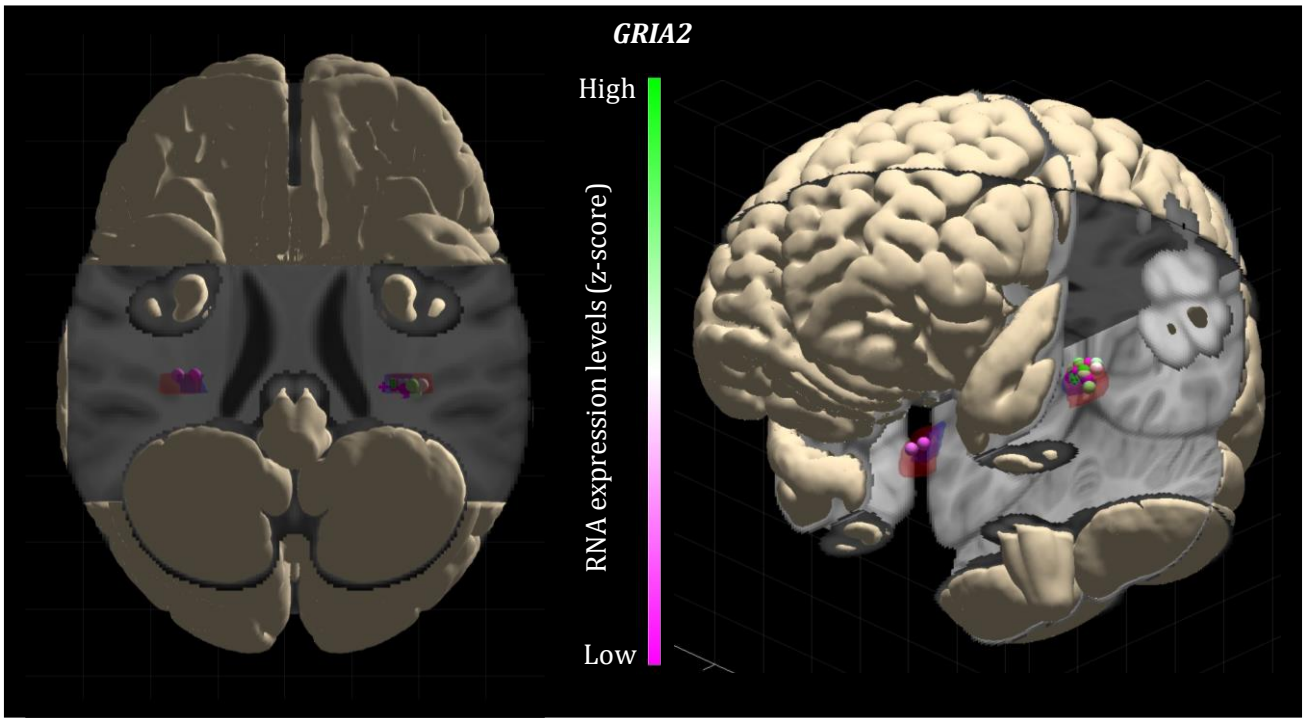

Supplementary Table S1. Protocols for receptor autoradiography.

Transmitter	Receptor (type/ mechanism)	Ligand[#] (L, K_D, Sa)	Property/ Exposure-time	Displacer	Incubation buffer	Pre-incubation	Main incubation	Final rinsing
Glutamate	AMPA (io / ex)	[^{3}H]-AMPA (9.92/10.0/55.7)	Agonist (15 weeks)	Quisqualate (10 µM)	50 mM Tris-acetate (pH 7.2) [+ 100 mM KSCN]*	3 x 10 min, 4 °C	45 min, 4 °C	1) 4 x 4 sec, 4 °C 2) Acetone/glutaraldehyde (950 ml + 50 ml), 2 x 2 sec, 22 °C
	NMDA (io / ex)	[^{3}H]-MK-801 (3.6/3.3/25.2)	Antagonist (12 weeks)	(+)MK-801 (100 µM)	50 mM Tris-HCl (pH 7.2) + 50 µM Glutamate [+30 µM Glycine + 50 µM Spermidine]*	15 min, 4 °C	60 min, 22 °C	1) 2 x 5 min, 4 °C 2) Distilled water, 1 x 1 dip, 4 °C
	Kainate (io / ex)	[^{3}H]-Kainate (9.9/12.0/46.9)	Agonist (12 weeks)	SYM 2081 (100 µM)	50 mM Tris-citrate (pH 7.1) [+10 mM Ca^{2+}-acetate]*	3 x 10 min, 4 °C	45 min, 4 °C	1) 3 x 4 sec, 4 °C 2) Acetone/glutaraldehyde (950 ml + 50 ml), 2 x 2 sec, 22 °C
	mGluR2/3 (me / ex)	[^{3}H]-LY 341,495 (1.13/4.0/60.0)	Antagonist (10 weeks)	L-Glutamate (1 mM)	10 mM Phosphate buffer (pH 7.6) [+ 100 mM KBr]*	2 x 5 min, 22 °C	60 min, 4 °C	1) 2 x 5 min, 4 °C 2) Distilled water, 1 x 1 dip, 4 °C
GABA	$GABA_A$ (io / in)	[^{3}H]-Muscimol (8.5/7.7/25.2)	Agonist (12 weeks)	GABA (10 µM)	50 mM Tris-citrate (pH 7.0)	3 x 5 min, 4 °C	40 min, 4 °C	1) 3 x 3 sec, 4 °C 2) Distilled water, 1 x 1 dip, 4 °C
	$GABA_A$/BZ (io / in)	[^{3}H]-Flumazenil (0.96/2.0/81.5)	Antagonist (9 weeks)	Clonazepam (2 µM)	170 mM Tris-HCl (pH 7.4)	15 min, 4 °C	60 min, 4 °C	1) 2 x 1 min, 4 °C 2) Distilled water, 1 x 1 dip, 4 °C
Acetylcholine	M_1 (me / ex)	[^{3}H]-Pirenzepine (7.84/3.0/83.8)	Antagonist (12 weeks)	Pirenzepine dihydrochloride (2 µM)	Modified Krebs-Buffer (pH 7.4)	15 min, 4 °C	60 min, 4 °C	1) 2 x 1 min, 4 °C 2) Distilled water, 1 x 1 dip, 4 °C
	M_2 (me / in)	[^{3}H]-Oxotremorine-M (1.73/0.8/82.0)	Agonist (15 weeks)	Carbachol (10 µM)	20 mM HEPES-Tris (pH 7.5) + 10 mM $MgCl_2 \times 6H_2O$	20 min, 22 °C	60 min, 22 °C	1) 2 x 2 min, 4 °C 2) Distilled water, 1 x 1 dip, 4 °C
	M_3 (me / ex)	[^{3}H]-4-DAMP (1.0/0.2/83.0)	Antagonist (9 weeks)	Atropine sulfate (10 µM)	50 mM Tris-HCl (pH 7.4) + 0.1 mM PMSF + 1 mM EDTA x $2H_2O$	15 min, 22 °C	45 min, 22 °C	1) 2 x 5 min, 4 °C 2) Distilled water, 1 x 1 dip, 4 °C
Noradrenaline	α_1 (me / ex)	[^{3}H]-Prazosin (0.22/0.2/77.4)	Antagonist (15 weeks)	Phentolamine Mesylate (10 µM)	50 mM Na/K-phosphate buffer (pH 7.4)	15 min, 22 °C	60 min, 22 °C	1) 2 x 5 min, 4 °C 2) Distilled water, 1 x 1 dip, 4 °C
Serotonin	$5\text{-}HT_{1A}$ (me / in)	[^{3}H]-8-OH-DPAT (0.97/2.0/162.0)	Agonist (15 weeks)	5-Hydroxy-Tryptamine (1 µM)	170 mM Tris-HCl (pH 7.7) [+ 4 mM $CaCl_2 \times 2H_2O$ + 0.01% Ascorbate]*	30 min, 22 °C	60 min, 22 °C	1) 1 x 5 min, 4 °C 2) Distilled water, 3 x 1 dips, 4 °C
	$5\text{-}HT_2$ (me / ex)	[^{3}H]-Ketanserin (1.38/0.5/60.0)	Antagonist (15 weeks)	Mianserin HCl (10 µM)	170 mM Tris-HCl (pH 7.7)	30 min, 22 °C	120 min, 22 °C	1) 2 x 10 min, 4 °C 2) Distilled water, 3 x 1 dips, 4 °C
Dopamine	D_1 (me / ex)	[^{3}H]-SCH 23390 (1.62/0.14/83.2)	Antagonist (15 weeks)	SKF 83566 (1 µM)	50 mM Tris-HCl (pH 7.4) + 120 mM NaCl + 5 mM KCl + 2 mM $CaCl_2 \times 2H_2O$ + 1 mM $MgCl_2 \times 6H_2O$ [+1 µM Mianserin]*	20 min, 22 °C	90 min, 22 °C	1) 2 x 10 min, 4 °C 2) Distilled water, 1 x 1 dip, 4 °C
Adenosine	A_1 (me / in)	[^{3}H]-DPCPX+Gpp(NH)p (0.95/0.5/137.0)	Agonist (10 weeks)	R-PIA (100 µM)	170 mM Tris-HCl (pH 7.4) + 2 Units/l Adenosine deaminase [+ 100 µM Gpp(NH)p]*	15 min, 4 °C	120 min, 22 °C	1) 2 x 5 min, 4 °C 2) Distilled water, 1 x 1 dip, 4 °C

[#] For the ligand, we provide information concerning the free concentration of the specific ligand during incubation (L, nM), the equilibrium dissociation constant of the specific ligand (K_D, nM), and the specific activity of the specific ligand (Sa, Ci/mmol). * shows the chemical only included in the main incubation. Abbreviation: io, ionotropic; me, metabotropic; in, inhibitory; and ex, excitatory.

Supplementary Table S2. Principal component analyses (PCA) for the receptor density and RNA expression data, respectively.

Receptor density data		RNA expression data	
Components	Explained variance (%)	Components	Explained variance (%)
1	51.9753	1	70.5633
2	27.9094	2	11.5469
3	12.2648	3	8.7426
4	5.8245	4	4.3352
5	1.5413	5	1.6529
6	0.2647	6	1.4272
7	0.1453	7	0.6182
8	0.0456	8	0.4958
9	0.0177	9	0.2552
10	0.0094	10	0.1820
11	0.0011	11	0.1181
12	0.0006	12	0.0626
13	0.0002		

The PCA were performed separately for the receptor density and RNA expression data, the four first principal components together were found to explain 95% of the variance from receptor and corresponding gene data, respectively.

Supplementary Table S3. Analysis of receptor density differences between CA and DG regions.

Receptors	Receptor density (fmol/mg)		LOOO-CV	*p*-value	Effect size	Statistical power
	CA	DG				
AMPA	603.71 ± 47.37	635.43 ± 68.49	0/14	0.3234	0.5386	0.1207
NMDA	4226.6 ± 534.6	3870.1 ± 157.0	0/14	0.1155	0.9046	0.3133
Kainate	604.00 ± 72.25	571.71 ± 82.71	0/14	0.4387	0.4158	0.0806
mGluR2/3	3182.0 ± 1102	4188.0 ± 1316	0/14	0.1411	0.8288	0.2649
$GABA_A$	5701.3 ± 1136	5025.3 ± 803.2	0/14	0.2134	0.6871	0.1858
$GABA_A$/BZ	5120.0 ± 901.4	6579.5 ± 961.9	1/12	0.0220	0.6578	0.1715
M_1	593.14 ± 51.06	589.43 ± 57.20	0/14	0.8990	0.0685	0.0202
M_2	205.43 ± 25.02	189.14 ± 25.14	0/14	0.2577	0.6494	0.1676
M_3	807.29 ± 111.7	763.71 ± 37.29	0/14	0.3667	0.5232	0.1151
α_1	1058.6 ± 216.4	3432.1 ± 425.6	**14/14**	**0.0009***	**7.0309**	**1.0000**
$5\text{-}HT_{1A}$	3621.7 ± 409.8	1783.1 ± 363.3	**14/14**	**0.0009***	**4.7481**	**1.0000**
$5\text{-}HT_2$	464.71 ± 34.58	551.71 ± 69.88	**14/14**	**0.0062***	**1.5782**	**0.7804**
D_1	363.00 ± 41.39	379.57 ± 46.61	0/14	0.4776	0.3759	0.0700
A_1	2888.6 ± 298.5	2141.9 ± 309.1	**14/14**	**0.0015***	**2.4574**	**0.9922**

Uncorrected *p*-values are shown. * indicates *p* values that remain significant after partial Bonferroni correction. The densities of $GABA_A$/BZ binding sites in one sample were outlier and excluded from further analysis. The LOOO-CV (leave-one-observation-out cross-validation) column provides information concerning the ratio of number of remaining significances to repeating number to assess the robustness of *p*-value. The small, medium, and large levels of the effect size are 0.2, 0.5, 0.8 respectively (Cohen, 1992). The threshold of effective statistical power is usually set at 0.8 (Charan and Kantharia, 2013).

Supplementary Table S4. Analysis of receptor-encoding gene expression between CA and DG regions.

Receptors	Genes	Gene expression level		LOOO-CV	*p*-value	Effect size	Statistical power
		CA	DG				
AMPA	*GRIA1*	94.09 ± 27.92	176.1 ± 18.41	**13/13**	**0.0021***	**3.4088**	**1.0000**
	GRIA2	301.1 ± 55.48	407.4 ± 31.31	**13/13**	**0.0058***	**2.3075**	**0.9742**
	GRIA3	101.9 ± 23.76	110.6 ± 13.02	0/13	0.4453	0.4440	0.0803
	GRIA4	31.92 ± 5.567	34.03 ± 4.385	0/13	0.4526	0.4163	0.0732
NMDA	*GRIN1*	64.92 ± 12.99	60.84 ± 12.59	0/13	0.5574	0.3183	0.0517
	GRIN2A	165.4 ± 37.80	222.7 ± 23.68	**9/13**	**0.0086***	**1.7827**	**0.8422**
	GRIN2B	352.2 ± 99.71	491.6 ± 50.77	1/13	0.0170	1.7173	0.8121
	GRIN2C	20.35 ± 3.444	19.04 ± 4.608	0/13	0.5606	0.3260	0.0532
	GRIN2D	2.957 ± 0.897	2.270 ± 0.600	0/13	0.1386	0.8849	0.2708
	GRIN3A	5.279 ± 2.448	3.340 ± 1.409	1/13	0.1135	0.9490	0.3102
Kainate	*GRIK1*	24.22 ± 6.864	14.34 ± 3.219	**5/13**	**0.0081***	**1.7925**	**0.8463**
	GRIK2	19.98 ± 3.480	23.42 ± 1.606	1/13	0.0507	1.2323	0.5056
	GRIK3	3.443 ± 2.204	1.380 ± 0.662	0/13	0.0379	1.2224	0.4985
	GRIK4	9.136 ± 1.387	13.82 ± 2.066	**13/13**	**0.0018***	**2.7061**	**0.9961**
	GRIK5	21.85 ± 6.211	39.23 ± 8.573	**13/13**	**0.0043***	**2.3549**	**0.9789**
mGluR2/3	*GRM2*	1.840 ± 1.299	3.947 ± 1.026	2/13	0.0139	1.7814	0.8416
	GRM3	57.97 ± 18.68	35.51 ± 4.996	1/13	0.0210	1.5815	0.7395
$GABA_A$	*GABRA1*	107.7 ± 26.33	84.95 ± 11.95	0/13	0.0796	1.0814	0.3985
and	*GABRA2*	73.00 ± 20.55	110.7 ± 14.46	**13/13**	**0.0073***	**2.0916**	**0.9404**
$GABA_A$/BZ	*GABRA3*	60.55 ± 17.99	45.41 ± 7.024	1/13	0.0851	1.0735	0.3930
	GABRA4	23.90 ± 5.853	32.45 ± 1.993	**13/13**	**0.0024***	**1.8870**	**0.8831**
	GABRA5	48.30 ± 13.06	87.55 ± 16.80	**13/13**	**0.0028***	**2.6380**	**0.9945**
	GABRA6	0.013 ± 0.034	0.175 ± 0.225	2/13	0.0323	1.0541	0.3797
	GABRB1	60.89 ± 4.831	76.79 ± 6.715	**13/13**	**0.0018***	**2.7575**	**0.9971**
	GABRB2	217.5 ± 50.09	188.9 ± 47.07	0/13	0.3121	0.5865	0.1257
	GABRB3	114.1 ± 22.15	175.8 ± 17.67	**13/13**	**0.0027***	**3.0510**	**0.9995**
	GABRD	36.60 ± 16.55	55.52 ± 19.15	0/13	0.0822	1.0641	0.3865
	GABRE	0.600 ± 0.352	0.432 ± 0.161	0/13	0.3353	0.5977	0.1299
	GABRG1	30.86 ± 5.441	34.50 ± 7.640	0/13	0.3346	0.5560	0.1147
	GABRG2	100.2 ± 14.84	146.7 ± 19.19	**13/13**	**0.0012***	**2.7455**	**0.9969**
	GABRG3	11.49 ± 1.774	9.562 ± 2.329	0/13	0.1184	0.9428	0.3063
	GABRQ	6.454 ± 2.084	34.44 ± 9.217	**13/13**	**0.0012***	**4.3706**	**1.0000**
	GABRR2	0.230 ± 0.184	0.178 ± 0.184	0/13	0.6192	0.2808	0.0449
M_1	*CHRM1*	20.10 ± 7.087	25.00 ± 3.858	0/13	0.1625	0.8368	0.2429
M_2	*CHRM2*	1.343 ± 0.493	0.373 ± 0.161	**13/13**	**0.0032***	**2.5512**	**0.9915**
M_3	*CHRM3*	51.67 ± 6.518	71.09 ± 10.42	**13/13**	**0.0031***	**2.2797**	**0.9711**
α_1	*ADRA1A*	1.864 ± 0.340	7.403 ± 2.937	**13/13**	**0.0012***	**2.7754**	**0.9973**
	ADRA1B	6.293 ± 3.684	26.79 ± 16.99	**13/13**	**0.0012***	**1.7409**	**0.8233**
	ADRA1D	7.790 ± 3.712	8.997 ± 2.645	0/13	0.4971	0.3689	0.0620
5-HT_{1A}	*HTR1A*	11.46 ± 6.075	7.367 ± 2.664	0/13	0.1653	0.8461	0.2482
5-HT_2	*HTR2A*	24.95 ± 7.721	13.99 ± 5.995	1/13	0.0255	1.5679	0.7315
D_1	*DRD1*	3.246 ± 1.707	1.725 ± 0.533	1/13	0.0215	1.1601	0.4539
A_1	*ADORA1*	28.74 ± 6.761	33.49 ± 7.890	0/13	0.2596	0.6508	0.1512

RNA data derived from the same tissue regions (same donors) as were used for the analyses of receptor density differences. $GABA_A$ and $GABA_A$/BZ share the same encoding genes. Uncorrected *p*-values are shown. * indicates *p* values that remain significant after partial Bonferroni correction. The LOOO-CV (leave-one-observation-out cross-validation) column provides information concerning the ratio of number of remaining significances to repeating number to assess the robustness of *p*-value. The small, medium, and large levels of the effect size are 0.2, 0.5, 0.8 respectively (Cohen, 1992). The threshold of effective statistical power is usually set at 0.8 (Charan and Kantharia, 2013).

Supplementary Table S5. Comparable analysis of receptor encoding gene differences between CA and DG regions using the JuGEx tool and Allen Human Brain Atlas data (Hawrylycz et al., 2015; Hawrylycz et al., 2012).

Receptors	Genes	Genes expressions		*p*-value
		CA	DG	
AMPA	*GRIA1*	2.0243	2.6950	0.0706
	GRIA2	1.3036	1.7287	0.2695
	GRIA3	0.9565	1.0245	0.6043
	GRIA4	-1.8673	-0.5178	**0.0004***
NMDA	*GRIN1*	0.7384	1.3468	0.2789
	GRIN2A	0.7221	1.1152	0.1203
	GRIN2B	1.2265	1.4223	0.8739
	GRIN2C	-0.2689	-0.1960	0.9013
	GRIN2D	-0.6068	-0.3376	0.5018
	GRIN3A	-0.5819	0.2096	0.0247
Kainate	*GRIK1*	-0.0383	-0.7318	0.4691
	GRIK2	-0.0840	1.0895	**0.0046***
	GRIK3	-2.1491	-1.6644	0.2998
	GRIK4	0.9106	1.2483	0.8285
	GRIK5	0.9651	1.9340	0.2200
mGluR2/3	*GRM2*	-0.0580	1.4497	**0.0019***
	GRM3	-1.5394	-1.0344	0.2617
$GABA_A$	*GABRA1*	-0.4840	-0.3972	0.6124
and	*GABRA2*	0.8138	0.9709	0.6971
$GABA_A$/BZ	*GABRA3*	1.0224	0.6126	0.1037
	GABRA4	0.0449	0.2756	0.2915
	GABRA5	1.2789	1.1119	0.1618
	GABRA6	-0.3384	-0.4793	0.3901
	GABRB1	0.5947	0.9256	0.6627
	GABRB2	-0.2776	0.3241	0.2092
	GABRB3	1.3434	1.9434	**0.0026***
	GABRD	-1.3512	-0.3027	0.0196
	GABRE	-0.4882	-0.5901	0.4990
	GABRG1	-0.3201	-0.1504	0.3409
	GABRG2	-0.0273	0.3743	0.4142
	GABRG3	-0.3692	-0.7755	0.0375
	GABRQ	0.8875	1.6584	0.4918
	GABRR2	-0.0235	-0.4470	0.2533
M_1	*CHRM1*	0.5090	0.4834	0.4210
M_2	*CHRM2*	-0.9220	-0.9277	0.8551
M_3	*CHRM3*	0.4236	-0.2905	0.2550
α_1	*ADRA1A*	-0.7244	2.9808	**0.0036***
	ADRA1B	-0.7581	0.9258	0.0203
	ADRA1D	1.3846	0.6145	0.2319
$5\text{-}HT_{1A}$	*HTR1A*	1.5185	0.9743	0.1774
$5\text{-}HT_2$	*HTR2A*	-0.0918	-0.6278	0.0246
D_1	*DRD1*	-0.3265	-0.9785	0.0146
A_1	*ADORA1*	-0.4523	0.0638	0.2104

For validation analysis, probabilistic maps from the Julich Brain Atlas were adjusted in an editor to best spatially match sampling in CA and DG. The data is z-score. $GABA_A$ and $GABA_A$/BZ share the same encoding genes. Uncorrected *p*-values from JuGEx are shown. * indicates *p* values that remain significant after partial Bonferroni correction.

Supplementary Table S6. Analysis of correlations between receptor and encoding genes.

Receptors	Genes	CA			DG		
		LOOO-CV	*r*-value	*p*-value	LOOO-CV	*r*-value	*p*-value
AMPA	*GRIA1*	0.5592	0.5714	0.2000	-0.0833	-0.0857	0.9194
	GRIA2	0.9184	0.9286	0.0067*	0.0833	0.0857	0.9194
	GRIA3	0.2735	0.2857	0.5560	0.1333	0.1429	0.8028
	GRIA4	-0.0367	-0.0357	0.9635	0.7500	0.7714	0.1028
NMDA	*GRIN1*	0.6653	0.6786	0.1095	0.6333	0.6571	0.1750
	GRIN2A	-0.1020	-0.1071	0.8397	-0.0333	-0.0286	1.0000
	GRIN2B	0.1755	0.1786	0.7131	0.7000	0.7143	0.1361
	GRIN2C	-0.0694	-0.0714	0.9063	0.1667	0.1429	0.8028
	GRIN2D	-0.1020	-0.1071	0.8397	0.8667	0.8857	0.0333
	GRIN3A	-0.1020	-0.1071	0.8397	0.5667	0.6000	0.2417
Kainate	*GRIK1*	0.5592	0.5714	0.2000	0.1333	0.1429	0.8028
	GRIK2	0.3796	0.3929	0.3956	0.0833	0.0857	0.9194
	GRIK3	0.2816	0.2857	0.5560	0.1333	0.1429	0.8028
	GRIK4	0.4204	0.4286	0.3536	-0.5333	-0.5429	0.2972
	GRIK5	-0.4204	-0.4286	0.3536	-0.1833	-0.2000	0.7139
mGluR2/3	*GRM2*	0.0367	0.0357	0.9635	0.0833	0.0857	0.9194
	GRM3	0.4857	0.5000	0.2667	0.4000	0.4286	0.4194
$GABA_A$	*GABRA1*	0.4531	0.4643	0.3024	0.2500	0.2571	0.6583
	GABRA2	-0.1347	-0.1429	0.7825	-0.3667	-0.3714	0.4972
	GABRA3	0.5592	0.5714	0.2000	-0.2500	-0.2571	0.6583
	GABRA4	-0.3469	-0.3571	0.4444	-0.3667	-0.3714	0.4972
	GABRA5	0.3469	0.3571	0.4444	0.5833	0.6000	0.2417
	GABRB1	-0.5102	-0.5357	0.2357	-0.1833	-0.2000	0.7139
	GABRB2	0.2082	0.2143	0.6615	0.2500	0.2571	0.6583
	GABRB3	0.4531	0.4643	0.3024	-0.1833	-0.2000	0.7139
	GABRD	0.1347	0.1429	0.7825	0.2000	0.2000	0.7139
	GABRG1	-0.4204	-0.4286	0.3536	-0.2500	-0.2571	0.6583
	GABRG2	0.8122	0.8214	0.0341	0.4167	0.4286	0.4194
	GABRG3	0.1102	0.1071	0.8397	0.0167	0.0286	1.0000
	GABRQ	-0.7388	-0.7500	0.0663	0.3000	0.3143	0.5639
$GABA_A$/BZ	*GABRA1*	0.3667	0.3714	0.4972	0.6833	0.7143	0.1361
	GABRA2	0.5667	0.6000	0.2417	0.3500	0.3714	0.4972
	GABRA3	0.1833	0.2000	0.7139	0.4667	0.4857	0.3556
	GABRA4	-0.0833	-0.0857	0.9194	0.5833	0.6000	0.2417
	GABRA5	0.3333	0.3714	0.4972	0.2500	0.2571	0.6583
	GABRB1	-0.2500	-0.2571	0.6583	-0.4667	-0.4857	0.3556
	GABRB2	0.1000	0.0857	0.9194	0.6833	0.7143	0.1361
	GABRB3	-0.1833	-0.2000	0.7139	0.4000	0.4286	0.4194
	GABRD	0.0167	0.0286	1.0000	0.8667	0.8857	0.0333
	GABRG1	-0.8167	-0.8286	0.0583	0.4167	0.4286	0.4194
	GABRG2	0.2500	0.2571	0.6583	0.7500	0.7714	0.1028
	GABRG3	-0.2500	-0.2571	0.6583	-0.0833	-0.0857	0.9194
	GABRQ	-0.6833	-0.7143	0.1361	0.2500	0.2571	0.6583
M_1	*CHRM1*	0.3796	0.3929	0.3956	0.6833	0.7143	0.1361
M_2	*CHRM2*	0.1429	0.1429	0.7825	-0.4167	-0.4286	0.4194
M_3	*CHRM3*	-0.0449	-0.0357	0.9635	-0.5333	-0.5429	0.2972
α_1	*ADRA1A*	0.3143	0.3214	0.4976	0.5333	0.5429	0.2972
	ADRA1B	0.2082	0.2143	0.6615	0.0833	0.0857	0.9194
	ADRA1D	-0.3551	-0.3571	0.4444	0.5333	0.5429	0.2972
5-HT_{1A}	*HTR1A*	0.2816	0.2857	0.5560	-0.0936	-0.0870	0.8667
5-HT_2	*HTR2A*	-0.3551	-0.3571	0.4444	-0.0167	-0.0286	1.0000
D_1	*DRD1*	-0.3143	-0.3214	0.4976	-0.5833	-0.6000	0.2417
A_1	*ADORA1*	0.1347	0.1429	0.7825	0.8167	0.8286	0.0583

Uncorrected *p*-values are shown. Significant uncorrected values highlighted in yellow. * indicate *p* value that remains significant after partial Bonferroni correction. The LOOO-CV (leave-one-observation-out cross-validation) column provides information concerning the mean value of correlation coefficient ($r_{Looo\text{-}cv}$) performed to assess the robustness of *r*-value.

Supplementary Table S7. Main subunit expression of ionotropic glutamatergic and GABAergic receptors in the human hippocampus.

Ionotropic receptor	Main subunits in human hippocampus	References
AMPA	$GluR_{1-3}$	Borges et al. (2003)
NMDA	GluN1, GluN2A, and GluN2B	Luján et al. (2005)
Kainate	$GluK_{1-5}$	Luján et al. (2005)
$GABA_A$	α_{1-3}, β_{2-3}, and γ_2	Luján et al. (2005); Chuang and Reddy (2018)

Supplementary Table S8. Detailed information of correlation coefficients between gene expression level and receptor density in **Supplementary Fig. S3A.** The receptor name represents the correlation coefficient between the density of that specific receptor type and the corresponding gene expression level. Note, that for the ionotropic receptors (AMPA, NMDA, kainate, and GABA) we averaged the expression levels of the main subunit gene for that receptor before running the correlation analysis (as specified in **Supplementary Table S7**). For the metabotropic α_1 receptor, we also averaged the expression levels of the genes coding for the α_{1A}, α_{1B} and α_{1C} subtypes, which cannot be distinguished with the radiolabeled ligand used in the present study.

Type	CA	DG
AMPA	0.8214	0.1429
NMDA	0.0000	0.2571
Kainate	0.1429	-0.2000
mGluR2/3	0.5000	0.3714
$GABA_A$	0.1786	0.0857
$GABA_A$/BZ	0.0857	0.7714
M_1	0.3929	0.7143
M_2	0.1429	-0.4286
M_3	-0.0357	-0.5429
α_1	0.1786	0.4286
5-HT_{1A}	0.2857	-0.0870
5-HT_2	-0.3571	-0.0286
D_1	-0.3214	-0.6000
A_1	0.1429	0.8286

Supplementary Table S9. Detailed information of identified genes in **Supplementary Fig. S4.**

Group	Genes
G-CA/DG	*GRIA1, GRIA2, GRIN2A, GRIK1, GRIK4, GRIK5, GABRA2, GABRA4, GABRA5, GABRB1, GABRB3, GABRG2, GABRQ, CHRM2, CHRM3, ADRA1A, ADRA1B*
G/R-CA	*GRIA1, GRIA2, GRIN1, GRIK1, GRIK4, GRIK5, GRM3, GABRA1, GABRA2, GABRA3, GABRB1, GABRB3, GABRG1, GABRG2, GABRQ*
G/R-DG	*GRIA4, GRIN1, GRIN2B, GRIN2D, GRIN3A, GRIK4, GRM3, GABRA1, GABRA3, GABRA4, GABRA5, GABRB1, GABRB2, GABRB3, GABRD, GABRG1, GABRG2, CHRM1, CHRM2, CHRM3, ADRA1A, ADRA1D, DRD1, ADORA1*

Abbreviations: G-CA/DG, 17 genes showing significantly different expression levels between CA and DG; G/R-CA, 15 genes presenting high-strength correlations with corresponding receptors in CA; and G/R-DG, 24 genes with high-strength correlations in DG. Abbreviation: G, gene; R, receptor.

Supplementary References:

Amunts, K., Mohlberg, H., Bludau, S., Zilles, K., 2020. Julich-Brain: A 3D probabilistic atlas of the human brain's cytoarchitecture. Science 369, 988-992.

Bludau, S., Mühleisen, T.W., Eickhoff, S.B., Hawrylycz, M.J., Cichon, S., Amunts, K., 2018. Integration of transcriptomic and cytoarchitectonic data implicates a role for MAOA and TAC1 in the limbic-cortical network. Brain Struct Funct 223, 2335-2342.

Borges, K., Myers, S.J., Zhang, S., Dingledine, R., 2003. Activity of the rat GluR4 promoter in transfected cortical neurons and glia. J Neurochem 86, 1162-1173.

Charan, J., Kantharia, N.D., 2013. How to calculate sample size in animal studies? J Pharmacol Pharmacother 4, 303-306.

Chuang, S.-H., Reddy, D.S., 2018. Genetic and Molecular Regulation of Extrasynaptic GABA-A Receptors in the Brain: Therapeutic Insights for Epilepsy. J Pharmacol Exp Ther 364, 180.

Cohen, J., 1992. A power primer. Psychol Bull 112, 155.

Hawrylycz, M., Miller, J.A., Menon, V., Feng, D., Dolbeare, T., Guillozet-Bongaarts, A.L., Jegga, A.G., Aronow, B.J., Lee, C.-K., Bernard, A., Glasser, M.F., Dierker, D.L., Menche, J., Szafer, A., Collman, F., Grange, P., Berman, K.A., Mihalas, S., Yao, Z., Stewart, L., Barabási, A.-L., Schulkin, J., Phillips, J., Ng, L., Dang, C., Haynor, D.R., Jones, A., Van Essen, D.C., Koch, C., Lein, E., 2015. Canonical genetic signatures of the adult human brain. Nat Neurosci 18, 1832-1844.

Hawrylycz, M.J., Lein, E.S., Guillozet-Bongaarts, A.L., Shen, E.H., Ng, L., Miller, J.A., van de Lagemaat, L.N., Smith, K.A., Ebbert, A., Riley, Z.L., Abajian, C., Beckmann, C.F., Bernard, A., Bertagnolli, D., Boe, A.F., Cartagena, P.M., Chakravarty, M.M., Chapin, M., Chong, J., Dalley, R.A., Daly, B.D., Dang, C., Datta, S., Dee, N., Dolbeare, T.A., Faber, V., Feng, D., Fowler, D.R., Goldy, J., Gregor, B.W., Haradon, Z., Haynor, D.R., Hohmann, J.G., Horvath, S., Howard, R.E., Jeromin, A., Jochim, J.M., Kinnunen, M., Lau, C., Lazarz, E.T., Lee, C., Lemon, T.A., Li, L., Li, Y., Morris, J.A., Overly, C.C., Parker, P.D., Parry, S.E., Reding, M., Royall, J.J., Schulkin, J., Sequeira, P.A., Slaughterbeck, C.R., Smith, S.C., Sodt, A.J., Sunkin, S.M., Swanson, B.E., Vawter, M.P., Williams, D., Wohnoutka, P., Zielke, H.R., Geschwind, D.H., Hof, P.R., Smith, S.M., Koch, C., Grant, S.G.N., Jones, A.R., 2012. An anatomically comprehensive atlas of the adult human brain transcriptome. Nature 489, 391-399.

Luján, R., Shigemoto, R., López-Bendito, G., 2005. Glutamate and GABA receptor signalling in the developing brain. Neuroscience 130, 567-580.

Palomero-Gallagher, N., Kedo, O., Mohlberg, H., Zilles, K., Amunts, K., 2020. Multimodal mapping and analysis of the cyto- and receptorarchitecture of the human hippocampus. Brain Struct Funct 225, 881-907.

Scholtens, L.H., Schmidt, R., de Reus, M.A., van den Heuvel, M.P., 2014. Linking Macroscale Graph Analytical Organization to Microscale Neuroarchitectonics in the Macaque Connectome. J Neurosci 34, 12192.